Title

Remodeled connexin 43 hemichannels alter cardiac excitability and promote arrhythmias

Journal

The Journal of General Physiology, 155(7)

ISSN

0022-1295

Authors

Lillo, Mauricio A

Muñoz, Manuel

Rhana, Paula

et al.

Publication Date

2023-07-03

DOI

10.1085/jgp.202213150

Peer reviewed

JGP Journal of General Physiology

ARTICLE

Remodeled connexin 43 hemichannels alter cardiac excitability and promote arrhythmias

Mauricio A. Lillo[1], Manuel Muñoz[2], Paula Rhana[2], Kelli Gaul-Muller[1], Jonathan Quan[2], Natalia Shirokova[1], Lai-Hua Xie[3], Luis Fernando Santana[2], Diego Fraidenraich[3], and Jorge E. Contreras[1,2]

Connexin-43 (Cx43) is the most abundant protein forming gap junction channels (GJCs) in cardiac ventricles. In multiple cardiac pathologies, including hypertrophy and heart failure, Cx43 is found remodeled at the lateral side of the intercalated discs of ventricular cardiomyocytes. Remodeling of Cx43 has been long linked to spontaneous ventricular arrhythmia, yet the mechanisms by which arrhythmias develop are still debated. Using a model of dystrophic cardiomyopathy, we previously showed that remodeled Cx43 function as aberrant hemichannels (non-forming GJCs) that alter cardiomyocyte excitability and, consequently, promote arrhythmias. Here, we aim to evaluate if opening of remodeled Cx43 can serve as a general mechanism to alter cardiac excitability independent of cellular dysfunction associated with a particular cardiomyopathy. To address this issue, we used a genetically modified Cx43 knock-in mouse (S3A) that promotes cardiac remodeling of Cx43 protein without apparent cardiac dysfunction. Importantly, when S3A mice were subjected to cardiac stress using the β-adrenergic agonist isoproterenol (Iso), they displayed acute and severe arrhythmias, which were not observed in WT mice. Pretreatment of S3A mice with the Cx43 hemichannel blocker, Gap19, prevented Iso-induced abnormal electrocardiographic behavior. At the cellular level, when compared with WT, Iso-treated S3A cardiomyocytes showed increased membrane permeability, greater plasma membrane depolarization, and Ca^{2+} overload, which likely caused prolonged action potentials, delayed after depolarizations, and triggered activity. All these cellular dysfunctions were also prevented by Cx43 hemichannel blockers. Our results support the notion that opening of remodeled Cx43 hemichannels, regardless of the type of cardiomyopathy, is sufficient to mediate cardiac-stress-induced arrhythmogenicity.

Introduction

The intercalated discs of healthy cardiomyocytes contain voltage-gated sodium and gap junction channels that are essential for cardiac conduction via ephaptic and electrotonic coupling (Kleber and Saffitz, 2014). Gap junction channels, in particular, act as low resistance channels that allow direct cytoplasmic communication between apposing cardiomyocytes. The connexin 43 (Cx43) gap junction–forming protein is the most abundant connexin in the heart and is found in the working myocardium of the atrium and ventricle as well as the more distal regions of the Purkinje network (Gutstein et al., 2001; Oxford et al., 2007; Kleber and Saffitz, 2014). Multiple inherited or acquired cardiomyopathies, including dystrophic muscle dysfunction, arrhythmogenic right ventricular cardiomyopathy (ARVC), ischemia/reperfusion, and hypertension, show an abnormal expression and remodeling of Cx43 (Severs et al., 2004a, 2004b, 2006; Oxford et al., 2007; Wang et al., 2013; Gonzalez et al., 2015, 2018; Kim et al., 2019; Himelman et al., 2020). This dysregulation is thought to play a meaningful mechanistic role in the evolution of lethal cardiac arrhythmias (Gonzalez et al., 2015; Kim et al., 2019; Lillo et al., 2019; Himelman et al., 2020), likely by affecting the appropriate generation and spread of cardiac action potentials (APs; Severs et al., 2006; Remo et al., 2011, 2012; Lillo et al., 2019)

A common pathological feature of Cx43 cardiac remodeling is the dephosphorylation of a triplet of serine residues S325/S328/S330 at the C-terminal domain of Cx43. These residues are usually phosphorylated by Ca^{2+}/calmodulin protein kinase II (CaMKII) and/or casein kinase 1δ (CK1δ), which is a critical step for proper Cx43 localization at the intercalated discs (Qu et al., 2009; Huang et al., 2011; Remo et al., 2011). This mechanism of remodeling is strongly supported by data from Cx43 knock-in mouse lines where the three serine residues (S325/S328/S330) were replaced by phosphomimetic glutamic acid (S3E) or by non-phosphorylatable alanines (S3A). The S3E mice subjected to

[1]Department of Pharmacology, Physiology and Neuroscience, Rutgers University, New Jersey Medical School, Newark, NJ, USA; [2]Department of Physiology and Membrane Biology, University of California, Davis. Davis, CA, USA; [3]Department of Cell Biology and Molecular Medicine, Rutgers University, New Jersey Medical School, Newark, NJ, USA.

Correspondence to Jorge E. Contreras: jecontrer@ucdavis.edu.

chronic pressure-overload hypertrophy were resistant to pathological Cx43 remodeling and to the induction of ventricular arrhythmias (Remo et al., 2011). Similarly, we showed that dystrophic mice containing S3E residues (mdxS3E) displayed an absence of Cx43 remodeling with improved intracellular Ca^{2+} signaling and ROS production (Himelman et al., 2020). In addition, mdxS3E mice were less susceptible to arrhythmias and to the development of cardiomyopathy (Himelman et al., 2020). On the other hand, S3A mice showed reduced gap junction formation and increased Cx43 remodeling in hearts subjected to chronic pressure-overload hypertrophy, consequently enhancing cardiac pathology (Remo et al., 2012; Himelman et al., 2020). Similar results were obtained for dystrophic mdxS3A mice. It was also shown that isolated hearts of S3A mice were more susceptible to inducible ventricular arrhythmias (Remo et al., 2011, 2012). Yet, the mechanisms by which they developed arrhythmias remain unclear (Remo et al., 2011, 2012).

Our group and others have recently proposed that remodeled Cx43 forms unpaired hemichannels (non-junctional channels) in ischemia and dystrophic mouse models (Wang et al., 2013; Gonzalez et al., 2018; Lillo et al., 2019; Himelman et al., 2020). Normally, unpaired Cx43 hemichannels are highly regulated to remain closed at the plasma membrane. However, we showed that mislocalized (lateralized) hemichannels in dystrophic mice are aberrantly activated upon cardiac stress leading to arrhythmias and sudden death (Gonzalez et al., 2015, 2018). We found that β-adrenergic stimulation induced ventricular arrhythmias in dystrophic mouse models (mdx mice) but not in WT mice. This effect is prevented by injecting connexin mimetic peptides that selectively block Cx43 hemichannels, but not GJ channels (Wang et al., 2013; Abudara et al., 2014; Gonzalez et al., 2015), or by genetically lowering levels of Cx43 (mdx:$Cx43^{+/-}$; Gonzalez et al., 2018). Similarly, in an ARVC mouse model where Cx43 is remodeled (Oxford et al., 2007; Kim et al., 2019), it has been shown that Cx43 hemichannels disrupt Ca^{2+} homeostasis, promoting lethal arrhythmogenesis (Kim et al., 2019). We discovered that β-adrenergic stimulation increases membrane permeability, depolarizes the plasma membrane, and promotes triggered activity (TA) in dystrophic isolated cardiomyocytes via the opening of S-nitrosylated lateralized Cx43 hemichannels (Lillo et al., 2019). While the evidence for remodeled Cx43 hemichannels in cardiac dysfunction is emerging, it is unknown whether hemichannel opening is associated with unique cellular dysfunctions characteristic of specific cardiomyopathy. For example, arrhythmias and sudden death are seen in mouse models of Duchenne muscular dystrophy; however, dystrophin loss and mechanical stress are present in addition to Cx43 remodeling.

Since Cx43 remodeling is observed in multiple cardiomyopathies, it is critical to explore whether the opening of Cx43 hemichannels and consequent alterations in membrane excitability serve as a general mechanism of cardiac dysfunction, independent of the etiology of the cardiomyopathy. To address this issue, we took advantage of the S3A mouse line, in which Cx43 remodeling is a result of direct genetic modification of the Cx43 protein rather than a consequence of cardiomyocyte pathological dysfunction. Upon cardiac stress, S3A mice developed acute ventricular arrhythmias consistent with previous observations in isolated hearts (Remo et al., 2011). In isolated S3A cardiomyocytes, β-adrenergic stimulation promoted membrane plasma depolarization and, subsequently, TA. These effects were prevented by blocking Cx43 hemichannels. Our data showed that the opening of remodeled Cx43 hemichannels is sufficient to promote cardiac-stress-induced arrhythmias.

Materials and methods

Mouse breeding and genotyping

S3A founder mouse colonies were a gift from Dr. Glenn Fishman (New York University, New York, NY). WT mice were purchased from Jackson Labs and examined at time points of 5–6 mo. All animal investigations were supported by the IACUC of Rutgers New Jersey Medical School and University of California Davis Medical School and performed following the National Institutes of Health guidelines.

Cardiomyocytes

Ventricular myocytes were enzymatically isolated from WT or S3A mice. Mice were heparinized (5,000 U/kg) and then anesthetized with overdosed isoflurane. The hearts were removed and perfused at 37°C in the Langendorff method with nominally Ca^{2+}-free Tyrode's solution containing 0.5 mg/ml collagenase (type II; Worthington) and 0.1 mg/ml protease (type XIV; Sigma-Aldrich) for 10 min. Ca^{2+}-free Tyrode's solution containing (in mM) 136 NaCl, 5.4 KCl, 0.33 NaH_2PO_4, 1 $MgCl_2$, 10 glucose, and 10 HEPES (pH 7.4, adjusted with NaOH). The enzyme solution was then washed out, and the hearts were removed from the perfusion equipment. Left ventricles were placed in Petri dishes and were smoothly teased apart with forceps. Then, the cardiomyocytes were filtered through nylon mesh. The Ca^{2+} concentration was gradually increased to 1.0 mM, and the cells were stored at room temperature and used within 8 h. Only cells from the left ventricular wall were used.

Electrophysiology

Cardiomyocytes were patch-clamped in the whole-cell configuration of the patch-clamp technique in the current-clamp or the voltage-clamp mode at 37°C. To record APs, patch pipettes (2–5 MΩ) were loaded with an internal solution containing (in mM) 110 K^+-aspartate, 30 KCl, 5 NaCl, 10 HEPES, 0.1 EGTA, 5 Mg-ATP, and 5 Na_2-creatine phosphates (pH 7.2, adjusted with KOH). Note, the recorded membrane potentials were not corrected for the patch pipette–bath liquid junction potential.

The myocytes were superfused with normal Tyrode's solution containing (in mM) 136 NaCl, 5.4 KCl, 0.33 NaH_2PO_4, 1 $CaCl_2$, 1 $MgCl_2$, 10 glucose, and 10 HEPES (pH 7.4, adjusted with NaOH). APs were obtained with 2-ms, 2–4-nA square pulses at multiple pacing cycle intervals (PCLs). We quantified DADs, TAs, and changes in the resting membrane potential induced by Iso or nitric oxide (NO) donors between 5 and 10 min after stimulation. The Gap19 peptide (232 ng/µl) and Cx43 antibody (2.5 ng/µl) were added to the pipette solution to block Cx43 hemichannel activity. We used two or three cardiomyocytes per isolated heart per condition.

The two electrode-voltage clamp (TEVC) technique in *Xenopus laevis* oocytes was used to test hemichannel currents from

homomeric channels formed by hCx43 and hCx43S3A. Connexin clones were purchased from Origene. Nhe1-linearized hCx43 and hCxCx43S3A were transcribed in vitro to cRNAs using the T7 Message Machine kit (Ambion). Electrophysiological data were collected using the Pclamp10 software. All recordings were made at room temperature (20–22°C). For Cx43 expressing oocytes, the recording solutions contained (in mM) 117 TEA and 5 HEPES, and the extracellular Ca^{2+} concentration was 0.2 mM (pH 7.4, adjusted with *N*-methyl-D-glucamine). Currents from oocytes were recorded 2 d after cRNA injection using a Warner OC-725 amplifier (Warner Instruments). Currents were sampled at 2 kHz and low-pass filtered at 0.5 kHz. Microelectrode resistances were between 0.1 and 1.2 MΩ when filled with 3 M KCl. Antisense oligonucleotides against Cx38 were injected into each oocyte to reduce the expression of endogenous Cx38 at 4 h after harvesting the oocytes (1 mg/ml; using the sequence from Ebihara [1996]). We assessed hemichannel currents and changes in the resting membrane potential evoked by NO 10 min after stimulation. We used at least three oocytes from each independent frog.

Field stimulation

APs were induced in isolated ventricular myocytes via field stimulation using two platinum wires (0.5 cm separation) placed at the bottom of the perfusion chamber. A Grass stimulator was used to generate square voltage pulses (4-ms duration) with an amplitude of 5–10 V at frequencies ranging from 0.5 to 2.0 Hz.

Confocal imaging of Ca^{2+} transients

Acutely isolated ventricular myocytes were loaded with the membrane-permeable acetoxymethyl-ester form of the Ca^{2+} indicator Fluo-4 (Fluo-4 AM) for the measurement of intracellular Ca^{2+} as previously described (Rossow et al., 2009). Experiments to measure AP-evoked whole-cell Ca^{2+} transients were performed on the stage of an Olympus FluoView 3000 confocal microscope using an Olympus APON (60×, NA = 1.49) oil-immersion lens. Briefly, a droplet of Fluo-4–loaded myocytes was added to a temperature-controlled chamber on the stage of the microscope containing a physiological Tyrode's solution. The cells were allowed to settle at the bottom of the chamber for 1–2 min before field stimulation was initiated. All experiments were performed at 37°C. We imaged Ca^{2+} transients using our confocal microscope in line-scan mode (2 ms/line). During analysis, background-subtracted fluorescence signals were normalized by dividing fluorescence at each point (F) with the baseline fluorescence (F_0). The amplitude kinetics of the spatially averaged $[Ca^{2+}]_i$ records were determined using pClamp 10.

Telemetry device implantation

A Data Sciences International (DSI) telemetry transmitter, used to perform electrocardiography, was inserted as follows: after the animal was anesthetized by isoflurane, shaved, and aseptically prepared, a 1–2 cm transverse incision was made in the left inguinal area. A subcutaneous pocket was created on the left side of the abdomen up toward the caudal edge of the rib cage. The telemetric transmitter, which is a tubular disk 1 cm in diameter × 2 cm in length, was inserted into the subcutaneous pocket and secured to the abdominal wall with sutures in three places on the left flank. Two ECG lead wires were tunneled subcutaneously; the ends were stripped to provide transmission and then coiled and secured to the underlying muscle tissue. The positive ECG lead wire was tunneled to the lower left rib cage and fixed to the abdominal muscle; the negative ECG lead was tunneled to the caudal end of the right scapula and fixed to the pectoralis muscle on the right side. Finally, the transverse inguinal incision was closed in two layers using interrupted mattress sutures and 3-0 nylon. This procedure does not require externalization of the wires, thus minimizing the possibility of infection and allowing the animal to be monitored without interference.

β-Adrenergic stress test recording

After recovering from telemetry device implantation surgery (3–5 d), mice were subjected to a 24-h Iso stress study. Mice were first weighed and separated into single cages that were placed on telemetry receivers. A 1-h baseline reading was taken to monitor activity and obtain ECG readings. Next, mice were intraperitoneally injected with Iso (I6504; isoproterenol, Sigma-Aldrich, 5 mg/kg). Mice were constantly recorded and observed for changes in activity and morbidity for 24 h. ECG data was analyzed by Lab Chart 8 software (Life Science Data Acquisition Software). Arrhythmias were scored based on a point system where: 0 = no arrhythmias, 1 = single premature ventricular contractions (PVCs), 2 = double PVCs, 3 = non-sustained ventricular tachycardia (VT), 4 = sustained VT or atrioventricular (AV) block, and 5 = death. We used between six and seven independent mice per experiment.

Dye perfusion and uptake in isolated hearts

Mice were heparinized (5,000 U/kg) and then anesthetized with isoflurane. Subsequently, mice were injected with either saline (control) or Iso (5 mg/kg, IP). 20 min after Iso or saline injection, mice were sacrificed and hearts were extracted and cannulated in a Langendorff perfusion system. Hearts were perfused with Normal Tyrode's (NT) buffer (in mM: 136 NaCl, 5.4 KCl, 0.33 NaH_2PO_4, 1 $MgCl_2$, 1 $CaCl_2$, 10 HEPES, and 10 glucose) at 37°C degrees for 10 min, followed by NT containing ethidium bromide (5 µM) or propidium iodide (50 µM) for 20 min and then NT buffer for 5 min to wash out the dye. Hearts were fixed overnight in 4% paraformaldehyde (Sigma-Aldrich), placed into 30% sucrose solution in PBS (Sigma-Aldrich) for 12 h, then embedded in O.C.T. (Tissue-Tek). Afterward, 10 µm cryosections were made, slides were thawed to room temperature, washed in PBS, and Alexa Fluor Wheat Germ Agglutinin 555 (Invitrogen) was applied for 20 min. Slides were then washed in PBS and mounted with a mounting reagent containing DAPI (Invitrogen). Slides were imaged using a 200 Axiovert fluorescence microscope (Zeiss). To calculate ethidium fluorescence in ImageJ, DAPI-stained nuclei were identified, created as ROI, and individual nuclei (100–150 per image) mean fluorescent intensities were measured. Then, the ROI outlines were projected onto the corresponding ethidium image, where individual fluorescent intensities were measured, capturing the ethidium signal within all nuclei. Ethidium intensity was then divided by DAPI nuclei intensity for each respective ROI signal,

then the mean ratio was calculated for all nuclei in the image. Three images per heart were evaluated in a blinded manner.

Biotin perfusion of isolated hearts

Mice were heparinized and then anesthetized with isoflurane. Once unconscious, mice were sacrificed and hearts were extracted and cannulated in a Langedorff perfusion system. Hearts were perfused with NT for 5 min, changed to NT buffer plus Biotin (EZ-Link NHS Biotin, 0.5 mg/ml, Thermo Fisher Scientific) for 60 min (0.25 ml/min flow rate), and washed out for 10 min with NT buffer plus 15 mM glycine. Left ventricular tissue was later homogenized in HEN buffer (in mM: 250 HEPES, 1 EDTA, and 0.1 neocuproine, pH 7.7) with 2× HALT protease inhibitors (Thermo Fisher Scientific) and then centrifuged at 16,000 *g* for 10 min. Following protein concentration determination, 50 µl of streptavidin beads (Thermo Fisher Scientific) were added to 200 µg protein and nutated for 90 min at 4°C with vortexing every 10 min. Samples were then centrifuged at 16,000 *g* for 2 min and the supernatant was dropped.

Next, the streptavidin pellet was resuspended in fresh lysis buffer containing 0.1% Triton X-100 and centrifuged for 1 min at 16,000 *g*. The pellet was then washed with PBS (pH 7.4) and centrifuged. 25 µl of 2× Laemmli sample buffer was added and heated at 100°C for 5 min to disrupt the biotin–streptavidin interaction. The heated samples were then centrifuged for 1 min at 16,000 *g* and the supernatant was run along with total protein extracts without streptavidin pulldown on SDS-PAGE.

Tissue immunofluorescence and Cx43 quantification

Immunofluorescent staining was performed on cryo-embedded cardiac sections with Cx43 (C6219; Sigma-Aldrich, 1:2,000, rabbit) and N-cadherin (33-3900, 1:400, mouse; Invitrogen) antibodies as described in Himelman et al. (2020). Confocal Z-stacks at a step size of 0.5 µm thickness (~12 slices per image) were acquired at 60× magnification on an Olympus Fluoview 1000 Confocal Laser Scanning Microscope using the Fluoview software. The Cx43/N-cadherin images were then separated into their separate channels and processed as maximum intensity z-stack projections in Fiji prior to analysis. Maximum intensity z-stacks were processed and Cx43 intensities at N-cadherin positive intercalated discs were calculated as described in Himelman et al. (2020).

Western blotting

Protein samples from the left ventricular heart wall or from injected *Xenopus* oocytes were separated by 10% SDS-PAGE and transferred onto a PVDF membrane (BioRad). The primary, Cx43 (#C8093; Sigma-Aldrich, 1:2,000, mouse), and secondary (Pierce; 1/5,000) antibodies were incubated using the Signal Enhancer HIKARI (Nacalai Tesque). Protein bands were detected with the SuperSignal West Femto (Pierce). Molecular mass was estimated with prestained markers (BioRad). Protein bands were analyzed using the ImageJ software (National Institutes of Health; NIH).

Detection of S-nitrosylated proteins

S-nitrosylated proteins were isolated from either mouse heart ventricular samples or *Xenopus* oocytes expressing Cx43 WT or Cx43SA. Heart tissue or *Xenopus* oocytes were homogenized in HEN buffer (in mM: 250 HEPES, 1 EDTA, and 0.1 Neucoproine, pH 7.7) containing protease inhibitors. Samples containing 200 µg protein were treated by the biotin-switch method to pull down all S-nitrosylated proteins as previously described (Lillo et al., 2019). S-nitrosylated proteins were separated using 10% SDS-PAGE and transferred onto a PVDF membrane (BioRad, Hercules). A monoclonal anti-Cx43 antibody (#C8093; 1:2,000, mouse; Sigma-Aldrich) was used to detect the Cx43 protein. For all Western blot analyses, the intensity of the signal was evaluated using ImageJ (NIH). We used six independent hearts per treatment.

Analysis of protein-to-protein association

The subcellular distribution and possible spatial association between S-NO and Cx43 were evaluated by Proximity Ligation Assay (PLA; Söderberg et al., 2006; Sigma-Aldrich). Tissue sections (6 µm) were blocked and incubated with two primary antibodies from different species, which were then detected using oligonucleotide-conjugated secondary antibodies as described in the manufacturer's protocols. Monoclonal anti-Cx43 (#C8093; 1:200; Sigma-Aldrich) and anti-S-nitrosocysteine (#N5411; 1:100; Sigma-Aldrich) antibodies were used. Images were visualized with a 200 Axiovert fluorescence microscope (Zeiss). We used five independent hearts per treatment. We quantified and analyzed the dots signal using ImageJ software and considered particle size of 0.3–10 μm^2, consistent with previous protocols procedures (López-Cano et al., 2019).

Chemicals

HEPES, cAMP, Na_2-creatine phosphate, K^+-aspartate, and *N*-methyl-D-glucamine were purchased from Sigma-Aldrich. Isoproterenol was obtained from Calbiochem and collagenase type II from Worthington. Gap19 was purchased from Tocris.

Statistical analysis

Values are displayed as mean ± standard error. Comparisons between groups were made using paired Student's *t* test, one-way ANOVA, or two-way ANOVA plus Tukey's post-hoc test, as appropriate. Electrophysiological and Ca^{2+} measurements in isolated cardiac cells (Figs. 3, 4, 5, and 7), when comparing results between WT and S3A cells from the same animal, were considered as technical replicates, and statistical comparisons were analyzed using a nested one-way ANOVA analysis as described (Eisner, 2021). $P < 0.05$ was considered significant. Each legend figure indicates the respective *n* value of the total mice used and the exact P value. In the case of $P < 0.0001$, we have added those as 0.0001. Statistical analyses were performed using GraphPad Prism 9.5.1 version and Origin 9 version.

Online supplemental material

Fig. S1 displayed the quantification of DADs (frequency and amplitude), TAs (frequency) in S3A isolated cardiomyocytes upon control conditions and under hyperpolarizing current injections with and without isoproterenol. Fig. S2 shows arrhythmogenic events in WT and S3A mice treated or not with a Cx43 hemichannels blocker (Gap 19) during light/dark cycle phase before and after a single isoproterenol injection.

Results

S3A knock-in mice displayed remodeling of Cx43 hemichannels

We reassessed the distribution of Cx43 in S3A knock-in mouse hearts. Previously, it was shown that there is a reduction of Cx43 in the intercalated discs of S3A mice (Remo et al., 2011, 2012); however, Cx43 hemichannel lateralization in the absence of cardiac pathological stimuli was not previously evaluated. To determine the distribution of Cx43 in WT and S3A hearts, we performed Cx43 immunohistochemistry in ventricular cryosections. Sections from 4–6-mo-old mice were stained against Cx43 (green) in conjunction with the intercalated disc marker, N-cadherin (red). Confocal immunofluorescence imaging revealed that Cx43 signal in WT cardiomyocytes is prominently confined at the intercalated discs, overlapping with N-cadherin (Fig. 1 A). Conversely, in S3A hearts, a substantial amount of Cx43 is found at the lateral side of cardiomyocytes, where it does not overlap with N-cadherin. Quantification of the relative Cx43 signal at the ID regions revealed that WT mice display significantly higher levels of Cx43 compared with S3A hearts (Fig. 1 A).

Next, we attempted to compare levels of lateralized Cx43 in cardiomyocytes from S3A versus WT hearts. To achieve this, we perfused isolated hearts from WT and S3A mice with cell-impermeable biotin (mol wt: 244.31), which strongly binds to non-junctional Cx43 hemichannels, as we have previously demonstrated (Lillo et al., 2019; Himelman et al., 2020). After aorta cannulation and biotin perfusion, hearts were homogenized, biotinylated proteins were pulled down with streptavidin beads, run on SDS-PAGE, and probed for Cx43. Western blot analysis of the biotinylated fraction showed that S3A hearts have nearly eightfold higher Cx43 protein levels at the lateral region compared with WT hearts. (Fig. 1 B). Both immunofluorescence and biochemical studies confirm that S3A cardiomyocytes display Cx43 remodeling as reported for various cardiac pathologies.

Iso-induced cardiac arrhythmias in S3A mice were prevented by blocking Cx43 hemichannels

We have previously shown that remodeled Cx43 protein mediates cardiac-stress-induced arrhythmias in dystrophic mice via the opening of Cx43 hemichannels (Gonzalez et al., 2018; Lillo et al., 2019; Himelman et al., 2020). Thus, we tested whether Cx43 remodeling in S3A mice leads to susceptibility to arrhythmias via a similar mechanism. We performed whole-animal ECGs using a telemetry system before and after Iso challenge in 4–6-mo-old WT and S3A mice under control condition or after pretreatment with the Cx43 hemichannel inhibitor, Gap19 (Wang et al., 2013; Abudara et al., 2014; 10 µg/kg via retroorbital injection). Representative ECGs recorded from WT and S3A mice treated with Gap19 are shown in Fig. 2 A. None of the mice in each group presented arrhythmias under baseline conditions. Following Iso administration, S3A mice developed severe arrhythmias, including PVCs, VT, and AV block (Fig. 2, A and B). In contrast, when pretreated with the Cx43 hemichannel blocker, Gap19, S3A mice displayed no abnormalities or very infrequent PVCs within 1 h post-Iso injection (Fig. 2, A and B). We further monitored arrhythmogenic behavior for 24 h following Iso stimulation in both WT and S3A mice. The S3A mice displayed increased arrhythmogenic events compared with WT mice within 24 h post-Iso injection (130.4 ± 4.5 and 10.2 ± 1.5, respectively; Fig. 2 C). The abnormal arrhythmogenic behavior detected in S3A mice was reduced following pretreatment with Gap19 (26.3 ± 6.2; Fig. 2 C).

Iso-induced opening of Cx43 hemichannels led to increased membrane permeability, Ca^{2+} overload, triggered activity, and prolonged APs in S3A cardiomyocytes

We previously showed that opening of remodeled Cx43 hemichannels increased membrane excitability and evoked triggered activity in Duchenne dystrophic isolated cardiomyocytes upon treatment with Iso (Lillo et al., 2019). Thus, we examined whether these pathological features are replicated in S3A cardiomyocytes. Fig. 3 A displays representative traces of cardiac APs from WT and S3A isolated cardiomyocytes induced by an injection of 2 nA current under current-clamp conditions. Electrically stimulated S3A isolated cardiomyocytes displayed an increase in the number (Fig. 3 B) and amplitude (Fig. 3 C) of delay after depolarizations (DADs) compared with WT cardiac cells, 37.0 ± 2.1 and 9.7 ± 2.3 per min, respectively. Treatment of cardiomyocytes with 1 µM Iso produced only an increased in amplitude (S3A: 8.76 ± 0.48; S3A + ISO: 11.8 ± 1.14), but not frequency (S3A: 37.0 ± 2.1; S3A + ISO: 27.7 ± 2.7) of DADs in S3A cardiomyocytes (Fig. 3, B and C). Consistently, S3A isolated cardiomyocytes showed a small increase in triggered activity (TA) compared with WT cardiac cells, 6.9 ± 0.99 and 2.4 ± 0.4 per minute, respectively (Fig. 3, A and B). Treatment of cells with 1 µM Iso-induced TA in S3A but not WT cardiomyocytes, 58.5 ± 4.6 and 2.86 ± 0.32 per minute, respectively (Fig. 3, A and B). To determine the role of Cx43 hemichannels in Iso-induced TA, we tested whether the addition of two different Cx43 hemichannel-specific blockers, Gap19 and Cx43 antibody (AbCx43; Lillo et al., 2019), into the patch pipette reduced DADs and TA. Iso-induced DADs and TA were significantly reduced by >70% in S3A cardiomyocytes treated with both Gap19 peptide (DADs = 3.04 ± 1.06 per minute; TA = 8.5 ± 0.6 per minute) and AbCx43 (DADs = 4.97 ± 1.09 per minute; TA = 4.8 ± 0.93 per minute; Fig. 3, A and B).

We next tested whether Iso-induced TA in S3A cardiomyocytes is correlated with alterations in the resting membrane potential (*Vm*), which in turn is produced by the distorted lateralized Cx43 hemichannels. Fig. 3 E shows that S3A cardiomyocytes are more depolarized with respect to WT cardiomyocytes under resting conditions, with *Vm* values of −64.9 ± 0.3 and −67.7 ± 0.52 mV, respectively. Furthermore, Iso stimulation depolarized both S3A and WT cardiomyocytes to *Vm* values of −61.6 ± 0.3 and −64.3 ± 0.36 mV, respectively (Fig. 3 C). Remarkably, when Cx43 hemichannels blockers (Gap19 or AbCx43) were included in the pipette solution, the *Vm* in S3A cardiomyocytes was restored to values similar to those observed in WT cardiac cells (Fig. 3 C). These results support that plasma membrane depolarization in S3A cardiomyocytes is caused by the disrupted activity of Cx43 hemichannels. To further demonstrate that Iso-induced depolarization of resting membrane potential plays a key role in generating DADs and TA in S3A cardiomyocytes, we injected hyperpolarizing currents to maintain the resting membrane potential near −68 mV (the values observed in WT cells

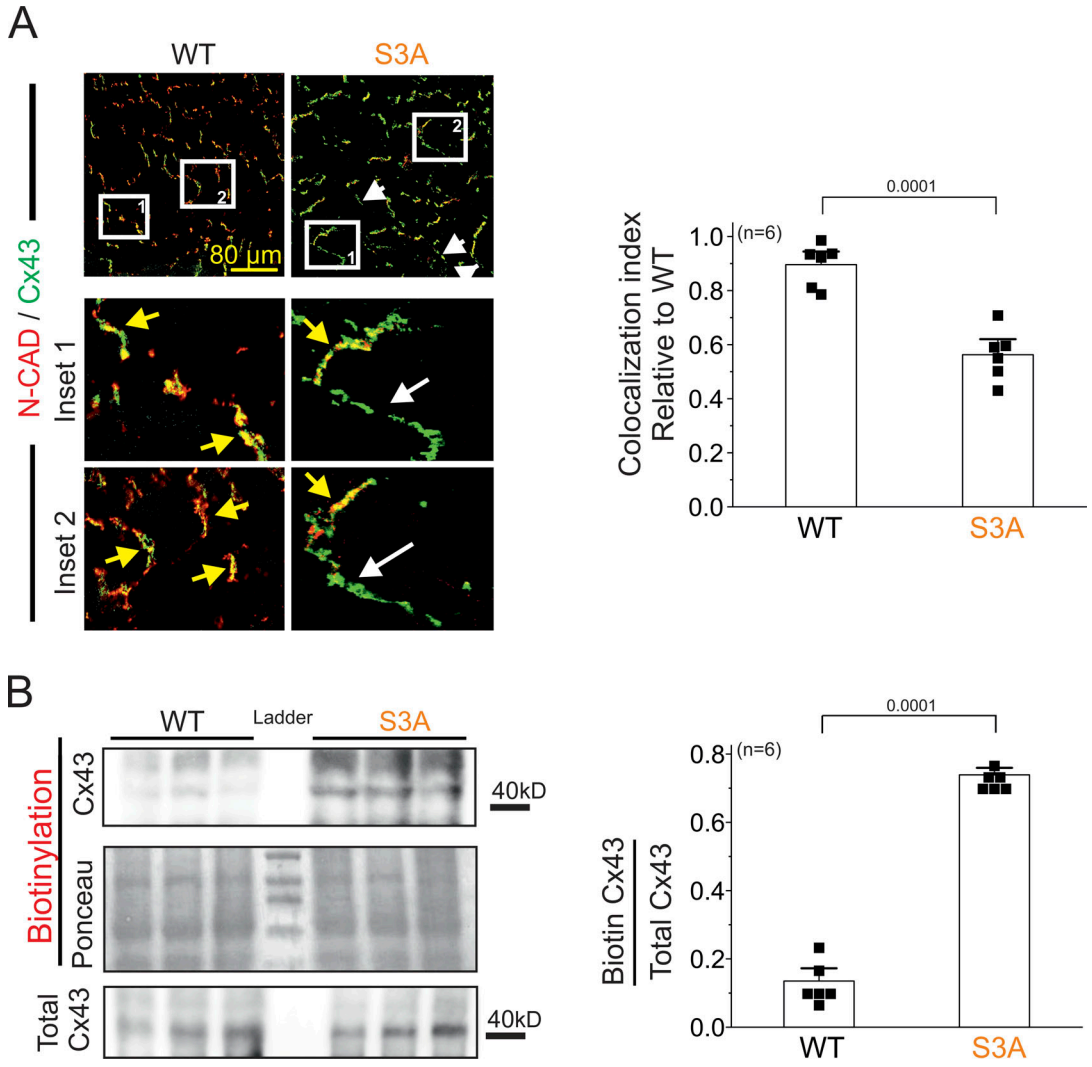

Figure 1. **Cx43 hemichannels are lateralized in cardiomyocytes of S3A mice. (A)** Representative confocal immunofluorescence images of cardiac intercalated discs and lateral regions of cardiomyocytes stained with Cx43 (green) and N-cadherin (red). Yellow and white arrows indicate the intercalated disc and lateral side, respectively. Right: Quantification of Cx43/N-cadherin colocalization in confocal immunofluorescence images. All data points were normalized to the WT group mean. Between three and five images containing 15–20 IDs were analyzed per heart. Each dot represents the mean value for each biological replicate. Comparisons between groups were made using Student's *t* test, P = 0.0001 vs. WT. The number in parentheses indicates the *n* total mice value. **(B)** Western blot analysis (left) and quantification (right) of Cx43 from biotin-perfused hearts (biotinylation). The bottom row represents Cx43-immunoblotted samples from heart lysates prior to pulldown (total Cx43). Biotinylated Cx43 levels were expressed as fold change relative to total Cx43 protein levels per sample. The number in parentheses indicates the *n* total mice value. Comparisons between groups were made using Student's *t* test, P = 0.0001 vs. WT. Source data are available for this figure: SourceData F1.

before Iso treatment). Hyperpolarizing current injections in S3A cardiomyocytes treated with Iso displayed a significant reduction in DADs amplitude and TA events (5.5 ± 0.5 and 2.3 0.2 ± 0.04 per min, respectively; Fig. S1).

Uptake from the extracellular space of hemichannel-permeable fluorescent molecules, such as ethidium bromide (EtBr), is generally used to identify the opening of Cx43 hemichannels (Contreras et al., 2003; Figueroa et al., 2013; Johnson et al., 2016). To confirm that Cx43 lateralized hemichannels are functional in S3A cardiomyocytes, we applied a semiquantitative in situ assay utilizing perfused isolated hearts, as previously reported (Lillo et al., 2019; Himelman et al., 2020). Under normal conditions, S3A hearts showed about fivefold greater EtBr uptake than WT hearts (Fig. 3 F). Iso stimulation enhanced EtBr uptake in both genotypes, but a significantly larger uptake was detected in S3A hearts (Fig. 3 F). In vivo treatment with Gap19 via retroorbital injection prior to Iso administration (5 mg/kg, IP) significantly reduced dye uptake in S3A hearts under both normal and Iso-stimulated conditions (Fig. 3 F).

Recent work has shown that the pathological opening of Cx43 hemichannels in cardiomyocytes leads to disruption of intracellular Ca^{2+} handling promoting Ca^{2+} overload (Gonzalez et al., 2018; Kim et al., 2019; De Smet et al., 2021). Thus, we examine whether the properties of intracellular Ca^{2+} transients evoked using field stimulation (1 Hz) are altered in S3A cardiomyocytes when compared with WT. Fig. 4 A shows representative confocal

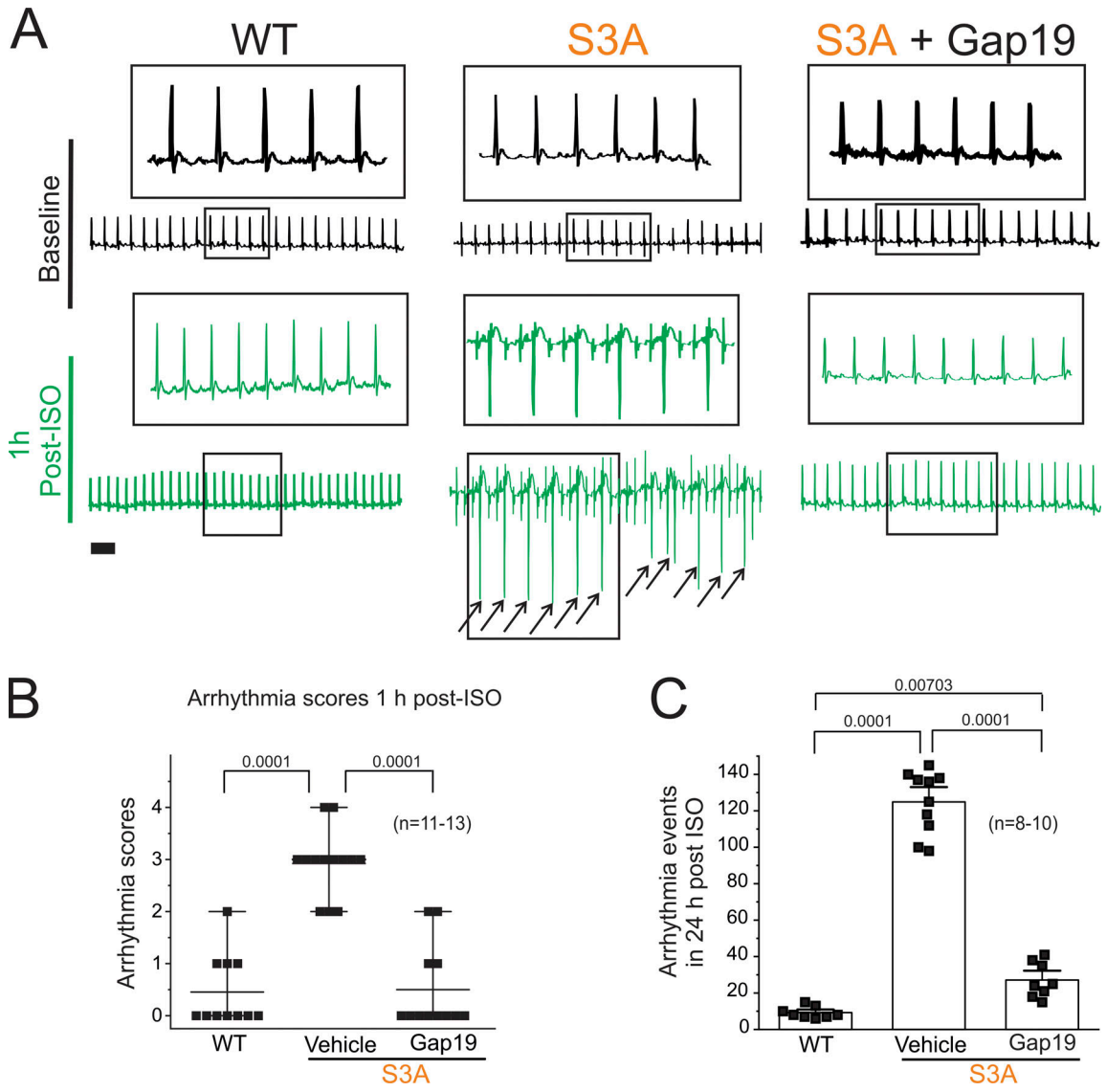

Figure 2. **β-adrenergic cardiac stress promotes arrhythmogenic phenotypes in S3A mice, which are prevented by blocking Cx43 hemichannels.** **(A)** Representative ECG traces obtained from 4–6-mo-old mice using an in vivo telemetry system in WT, S3A, and S3A mice treated with Gap19 via retroorbital injection (10 µg/kg). Scale bar is 100 ms for all traces. Black arrows indicate PVC arrhythmia events. **(B)** Arrhythmia scores 1-h post-Iso challenge based on a predetermined scale where 0 = no arrhythmias, 1 = single PVCs, 2 = double PVCs, 3 = triple PVCs or non-sustained VT, 4 = sustained VT or AV block, 5 = death. Comparisons between groups were made using two-way ANOVA plus Tukey's post-hoc test, P = 0.0001 WT vs. S3A; P = 0.0001 S3A vs. S3A + Gap19. The number in parentheses indicates biological replicates. **(C)** Quantification of arrhythmogenic events (including PVC, double PVC, VT, or AV block) during the 24 h post-Iso challenge in WT, S3A, and S3A mice treated with Gap19 via retroorbital injection (10 µg/kg). P = 0.0001 WT vs. S3A; P = 0.0001 S3A vs. S3A + Gap19; P = 0.00703 WT vs. S3A + Gap19. The number in parentheses indicates biological replicates. Comparisons between groups were made using two-way ANOVA plus Tukey's post-hoc test.

line-scan images of Ca^{2+} transients from WT (top) and S3A (bottom) cardiomyocytes in the absence and presence of Gap19 (Fig. 4 B). At basal conditions, the amplitude of Ca^{2+} transients was not significantly different between S3A and WT cardiomyocytes (Fig. 4 C). However, S3A cardiomyocytes displayed prolonged Ca^{2+} transient decays (87.82 ± 8.24 ms) compared with WT cardiomyocytes (60.24 ± 5.77 ms; Fig. 4 D). Pretreatment with Gap19 normalized Ca^{2+} transient decays in S3A cardiomyocytes (49.80 ± 8.49 ms) to similar values observed in WT (Fig. 4 D). Then, we analyzed the effect of Iso in S3A and WT cardiomyocytes nontreated or pretreated with GAP19. Fig. 5 A shows representative confocal line-scan images for a WT and a S3A cardiomyocyte before (black line) and after Iso (green line); while Fig. 5 B corresponds to representative images for WT and S3A cardiomyocytes pretreated with Gap19. Overall, Ca^{2+} transits amplitude did not display significant differences between S3A and WT cardiomyocytes when treated or not with Gap 19 (Fig. 5 C). Conversely, Ca^{2+} decay times were reduced in S3A cardiomyocytes pretreated with Gap19 in the presence of Iso (45.87 ± 7.86 ms) to those levels observed in WT cardiomyocytes with equivalent treatment (32.90 ± 3.63 ms; Fig. 5 D).

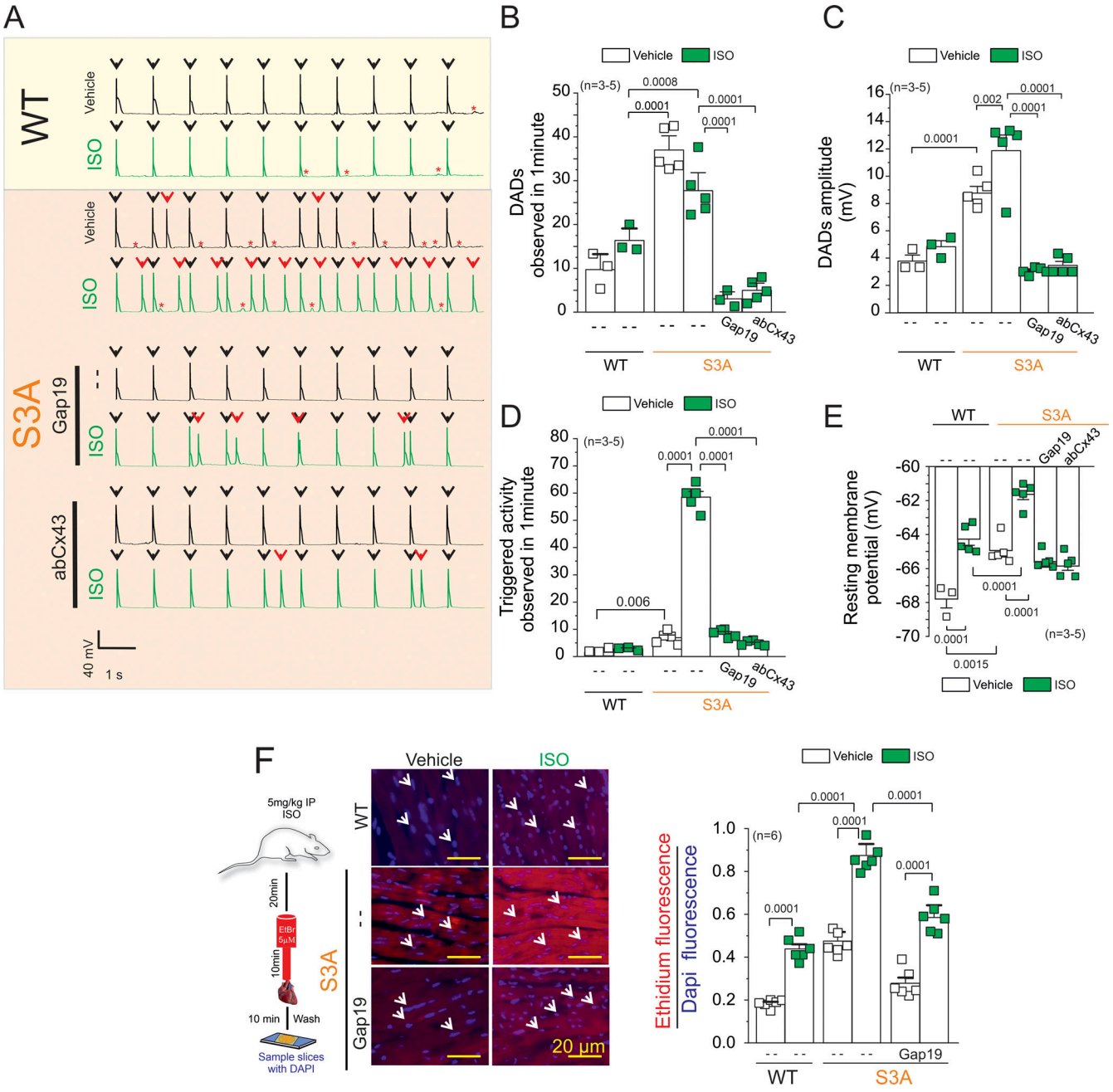

Figure 3. **Isoproterenol induces TA in S3A cardiomyocytes via the opening of Cx43 hemichannels. (A)** Representative AP traces of WT and S3A isolated cardiomyocytes. Cells were stimulated with 1 µM Iso (green) in the absence or presence of Cx43 blockers contained inside the pipette: Gap19 (232 ng/µl) and Cx43 antibody (abCx43; 2.5 ng/µl). Black arrows indicate electrical stimulation pulse. Red arrows indicate TAs. Red asterisks display DADs. **(B)** Quantification of DADs observed in A. P = 0.0001 WT + Iso vs. S3A; P = 0.0008 WT + Iso vs. .S3A + Iso; P = 0.0001 S3A + Iso vs. S3A + Iso + Gap19 and S3A + Iso + abCx43. Comparisons between groups were made using nested-ANOVA plus Tukey's post-hoc test. The number in parentheses indicates biological replicates. We analyzed three to five cells per mouse. **(C)** Quantification of DADs amplitude observed in A. P = 0.0001 WT vs. S3A; P = 0.002 S3A vs. S3A + Iso; P = 0.0001 S3A + Iso vs. S3A + Iso + Gap19 and S3A + Iso + abCx43. Comparisons between groups were made using nested-ANOVA plus Tukey's post-hoc test. The number in parentheses indicates biological replicates. We analyzed three to five cells per mouse. **(D)** Quantification of TA observed in A. Comparisons between groups were made using nested-ANOVA plus Tukey's post-hoc test. The number in parentheses indicates biological replicates. We analyzed three to five cells per mouse. P = 0.006 WT vs. S3A; P = 0.0001 S3A vs. S3A + Iso; P = 0.0001 S3A + Iso vs. S3A + Iso + Gap19 and S3A + Iso + abCx43. **(E)** Resting membrane potential of WT and S3A cardiomyocytes. The number in parentheses indicates the *n* total mice value. We analyzed three to five cells per mouse. P = 0.0001 WT vs. WT + Iso; P = 0.0015 WT vs. S3A; P = 0.0001 WT + Iso vs. S3A + Iso; P = 0.0001 S3A vs. S3A + Iso. Comparisons between groups were made using nested-ANOVA plus Tukey's post-hoc test. **(F)** Evaluation of Cx43 hemichannel activity in the whole heart via ethidium uptake. Isolated hearts were perfused with buffer containing 5 µM ethidium after vehicle or Iso (5 mg/kg, IP). The number in parentheses indicates biological replicate. P = 0.0001 WT vs. WT + Iso; P = 0.0001 WT + Iso vs. S3A + Iso; P = 0.0001 S3A vs. S3A + Iso; P = 0.0001 S3A + Iso vs. S3A + Iso + Gap19. Comparisons between groups were made using two-way ANOVA plus Tukey's post-hoc test.

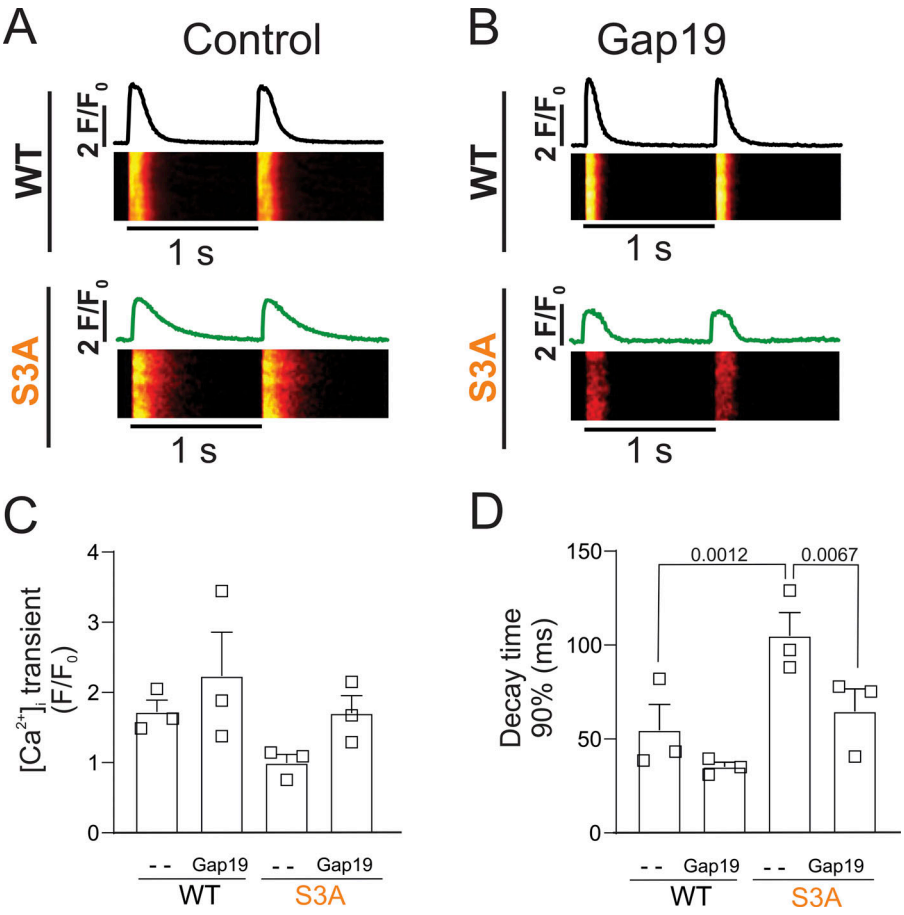

Figure 4. **S3A cardiomyocytes show an increased duration of $[Ca^{2+}]_i$ transients compared to WT cardiomyocytes, which was prevented by Cx43 hemichannel blockade. (A and B)** Representative line scan images from WT (top) and S3A (bottom) myocytes under field stimulation (1 Hz) in control conditions (A) and after incubation with Gap19 peptide (200 µM; B). The traces above each line scan represent the spatially averaged time curse of $[Ca^{2+}]_i$ for each image. The number in parentheses indicates biological replicates. We analyzed three to five cells per mouse. **(C and D)** Amplitude quantification (C) and decay time 90% (ms) quantification (D). The number in parentheses indicates the *n* value. P = 0.0012 WT vs. S3A; P = 0.0067 S3A vs. S3A + Gap19. Comparisons between groups were made using nested-ANOVA. The number in parentheses indicates biological replicates. We analyzed three to five cells per mouse.

Previous work has shown a significant increase in AP duration (APD) dispersion in S3A mice compared with WT (Remo et al., 2011). Thus, we analyzed whether specifically Cx43 hemichannels could alter APD interval in isolated cardiomyocytes from WT and S3A mice before and after treatment with 1 µM Iso. Consistent with previous findings (Lillo et al., 2019), S3A cardiomyocytes displayed longer APD with respect to WT cardiomyocytes under vehicle conditions, with APD values of 133.28 ± 3.3 ms and 104.8 ± 1.4 ms, respectively (Fig. 6, A and B). Furthermore, Iso stimulation increased both S3A and WT cardiomyocytes to APD values of 180.6 ± 3.3 ms and 134.83 ± 1.86 ms, respectively. When Cx43 hemichannels blockers (Gap19 or AbCx43) were contained in the pipette solution, APD in S3A cardiomyocytes was restored to values similar to those observed in WT cardiac cells (Fig. 6 B). These results indicate that the activity of Cx43 hemichannels influences APD in S3A cardiomyocytes. The fact that remodeled Cx43 hemichannels significantly alter the excitatory properties of cardiomyocytes is consistent with a role in conferring the proarrhythmic phenotype observed in these mice.

β-adrenergic cardiac stress evokes triggered activity in S3A cardiac cells via S-nitrosylation of lateralized Cx43 hemichannels

We recently reported that Iso-induced membrane depolarization and TA in the dystrophic cardiomyocytes required NO production and S-nitrosylation of Cx43 (Lillo et al., 2019). Therefore, we evaluated (1) whether direct stimulation of S3A cardiomyocytes with a NO donor, sodium 2-(N, N-diethylamino)-diazenolate-2-oxide (DEENO, 1 µM), can mimic Iso-induced disruption of membrane excitability and (2) whether Iso-induced disruption of membrane excitability is prevented by inhibition of NO production with NG-nitro-L-arginine methyl ester (L-NAME, 100 µM; Pfeiffer et al., 1996). Fig. 7 A shows representative APs in S3A isolated cardiomyocytes that were evoked by electrical stimulation in the absence or presence of Iso (1 µM), in the presence of 1 µM DEENO, or when S3A cardiomyocytes were pretreated with 100 µM L-NAME. Exogenous application of NO using DEENO does not significantly change the number and amplitude of DADs (33.5 ± 2.95 and 13.2 ± 0.12, respectively) when compared with vehicle (30.2 ± 1.1 and 9.3 ± 1.1) or Iso-treated S3A cardiomyocytes (29.8 ± 0.02 and 15.8 ± 2.5; Fig. 7, B and C). Nevertheless, DEENO increased TAs (58.5 ± 2.1) when compared with vehicle S3A treated cardiomyocytes (6.9 ± 0.9), resembling what is observed with Iso-treatment (58.5 ± 2.07; Fig. 7 D). Consistently, DEENO depolarized the membrane S3A cardiomyocytes (*Vm* of −61.8 ± 2.6) to similar values to those observed by Iso-treatment (values; Fig. 7 E). Inhibition of NO production with L-NAME significantly decreases the frequency (5.02 ± 0.75) and amplitude (3.4 ± 0.18) of DADs in both vehicle or Iso-treated S3A cardiomyocytes (Fig. 7, B and C). In addition, L-NAME treatment greatly reduced the incidence of Iso-evoked TAs in S3A cardiomyocytes (5.03 ± 0.75 per min) when compared with those that were vehicle treated (Fig. 7 D).

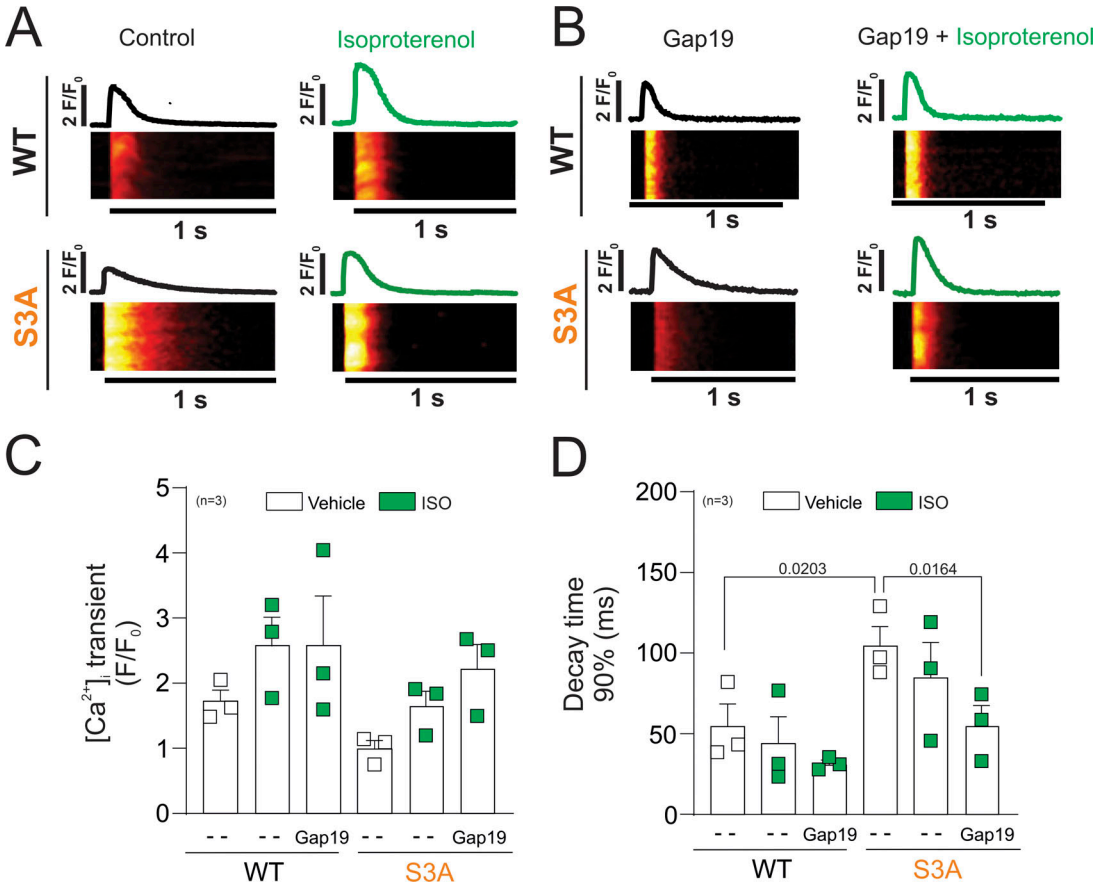

Figure 5. **Activation of β-adrenergic signaling decreases the duration of $[Ca^{2+}]_i$ transients in S3A cardiomyocytes treated with Gap19. (A)** Line scan images from representative WT (top) and S3A (bottom) cardiomyocytes under field stimulation (1 Hz) under control conditions (left) and after isoproterenol stimulation (right). **(B)** Line scan images from representative cardiomyocytes previously loaded with the Gap19 peptide (200 µM) before (left) and after (right) Iso stimulation (green). The traces above each line scan represent the spatially averaged time curse of $[Ca^{2+}]_i$ for each image. The number in parentheses indicates biological replicates. **(C and D)** We analyzed three to five cells per mouse. C and D show scatter plots of the amplitude and time to 90% decay, respectively. P = 0.0203 WT vs. S3A; P = 0.0164 S3A vs. S3A + Iso + Gap19. The number in parentheses indicates the *n* value. Comparisons between groups were made using nested-ANOVA. The number in parentheses indicates biological replicate. We analyzed three to five cells per mice.

Consistently, L-NAME treatment significantly reduced the Iso-induced decrease in resting membrane potential of S3A cardiomyocytes and restored it to similar values observed in WT cardiomyocytes (S3A: −64.2 ± 0.36; Iso: −61.4 ± 0.5; S3A + L-NAME: −68.12 ± 0.14, S3A + L-NAME + Iso: −67.8 ± 0.2; Fig. 7 E). These results support the notion that Iso-induced Cx43 hemichannels aberrant electrical activity in S3A cardiomyocytes via NO production.

To confirm that S3A mutations do not alter the NO response and biophysical properties of Cx43, we assessed Cx43S3A hemichannel currents in *Xenopus* oocytes using the TEVC technique. As we previously reported (Lillo et al., 2019), in the absence of NO donors, the voltage-activated leak currents in Cx43-expressing oocytes are similar to those observed in non-injected oocytes. However, the application of 10 µM DEENO evoked an increase in plasma membrane conductance at positive and negative voltages in Cx43-expressing oocytes but not in non-injected oocytes (Fig. 7 F). Oocytes expressing Cx43S3A mutations also displayed an increase in leak currents in response to DEENO (Fig. 7 F, orange box). NO-induced leak currents in Cx43S3A expressing oocytes were reduced in oocytes that were intracellularly injected with Cx43 hemichannel blockers, Gap19, or AbCx43 (Fig. 7 F, orange box). The increase in NO-induced leak currents was 2- and 1.6-fold in Cx43 and Cx43S3A expressing oocytes, respectively (Fig. 7 G). In addition, we found that NO evoked a more depolarized *Vm* in oocytes expressing Cx43 and Cx43S3A when compared with non-injected oocytes (Fig. 7 H). Inhibition of Cx43 hemichannels with Gap19 or AbCx43 prevented NO-induced *Vm* depolarization in Cx43S3A expressing oocytes (Fig. 7 H). Our results confirm that Cx43S3A hemichannels are activated by NO and result in resting membrane depolarization in *Xenopus* oocytes, which is similar to what was reported above for isolated S3A cardiomyocytes.

To evaluate the Cx43 S-nitrosylation status on S3A cardiac tissue, we used the PLA using antibodies that recognize S-nitrosylated proteins (S-NO) and the C-terminus of Cx43, as we have previously described (Lillo et al., 2019). We detected Cx43-NO signals (red stain) in the intercalated disc in both WT and S3A cardiac tissue under vehicle conditions (Fig. 8 A). S-nitrosylated levels of Cx43 were increased after treatment with Iso in both WT and S3A cardiac tissue (Fig. 8, A and B). At least 20% of the PLA signals are located at the lateral side of

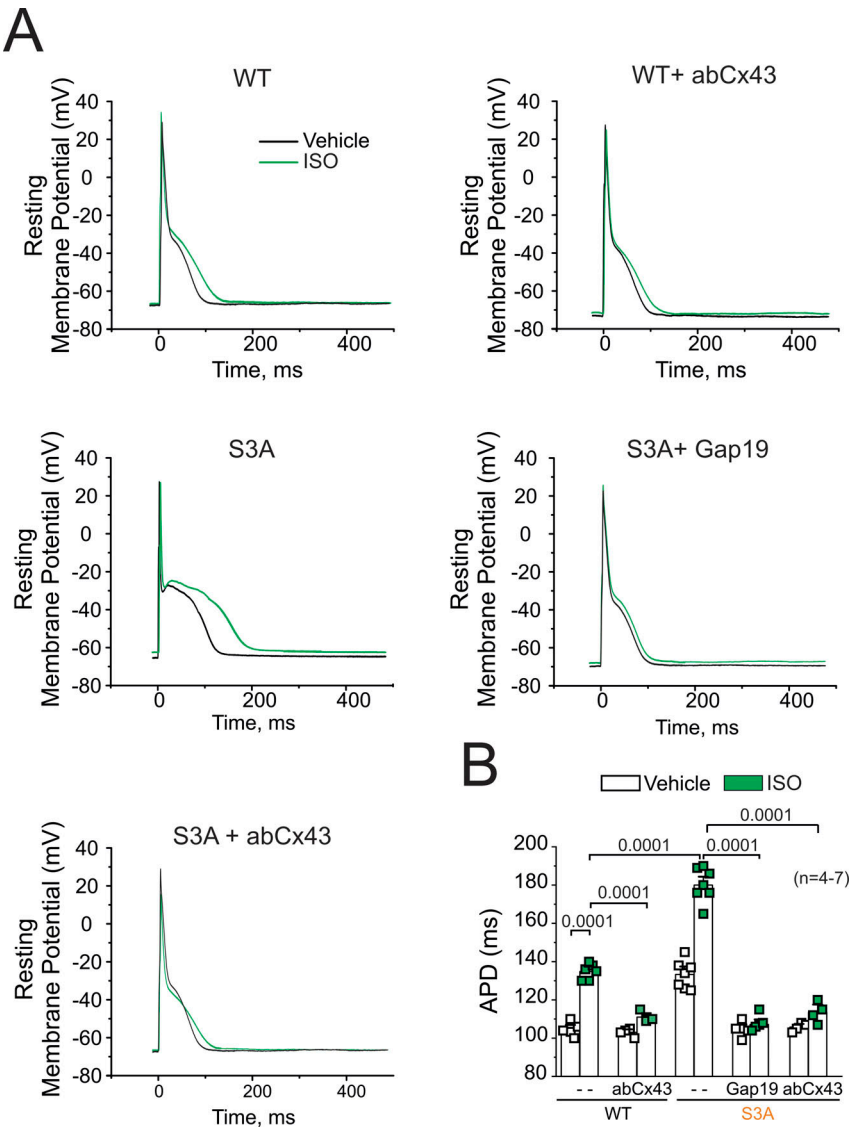

Figure 6. **Cx43 hemichannels are involved in APD prolongation in WT and S3A isolated cardiomyocytes. (A)** Representative AP traces of WT and S3A isolated cardiomyocytes. Cells were stimulated with 1 µM Iso (green) in the absence or presence of Cx43 blockers contained inside the pipette: Gap19 (232 ng/µl) and Cx43 CT antibody (abCx43; 2.5 ng/µl). **(B)** Quantification of APD observed in A. P = 0.0001 WT vs. WT + Iso; P = 0.0001 WT + Iso vs. WT + Iso + abCx43, P = 0.0001 WT + Iso vs. S3A + Iso, P = 0.0001 S3A + Iso vs. S3A + Iso + Gap19 and S3A + Iso + abCx43. Comparisons between groups were made using nested-ANOVA. The number in parentheses indicates biological replicate. We analyzed three to five cells per mouse.

cardiomyocytes in S3A hearts upon ISO stimulation (Fig. 8 C). These values are not affected by the size of the cardiac cells since WT and S3A have similar cell areas of ~2,000 µm² (Fig. 8 D). In addition, we used the biotin switch assay to corroborate differences in Cx43 S-nitrosylation levels between WT and S3A hearts. We found that levels of S-nitrosylated Cx43 in S3A cardiac tissue are close to twofold greater than in the WT heart under control conditions (Fig. 8 E). In vivo Iso treatment resulted in an increase in levels of S-nitrosylated Cx43 in both WT and S3A hearts by about two- and fourfold when compared with their respective controls (Fig. 8 E).

Discussion

Cx43 remodeling is well-accepted as a feature of cardiac pathologies involving spontaneous ventricular arrhythmia. In prior studies, we described that remodeled Cx43 forms undocked connexin hemichannels, whose activity leads to arrhythmias and cardiac dysfunction in a mouse model of Duchenne muscular dystrophy (Gonzalez et al., 2018; Lillo et al., 2019; Himelman et al., 2020). Here, we examine whether the opening of remodeled Cx43 hemichannels serves as a general mechanism underlying dysfunctional cardiomyocyte excitability or it is a pathologically dependent phenomenon. Using the S3A knock-in mice with genetically engineered remodeled Cx43 proteins, we showed that Iso-induced cardiac stress promoted a substantial number of arrhythmogenic events that were prevented by the blockade of Cx43 hemichannels. At the cellular level, we found that the blockade of Cx43 hemichannels prevents abnormal changes in membrane permeability, plasma membrane depolarization, and Iso-evoked DADs and TA. Our data are consistent with the idea that the opening of Cx43 hemichannels is, at least, one of the mechanisms by which Cx43 protein remodeling is involved in the development of arrhythmias.

Cx43 remodeling is observed in pathologic studies of human hearts with a broad class of collected arrhythmic symptoms, including ischemic and hypertrophic cardiomyopathies, acquired diseases such as arrhythmogenic right ventricular cardiomyopathy (ARVC), genetic diseases associated with somatic or germline mutations in connexin genes, and muscular

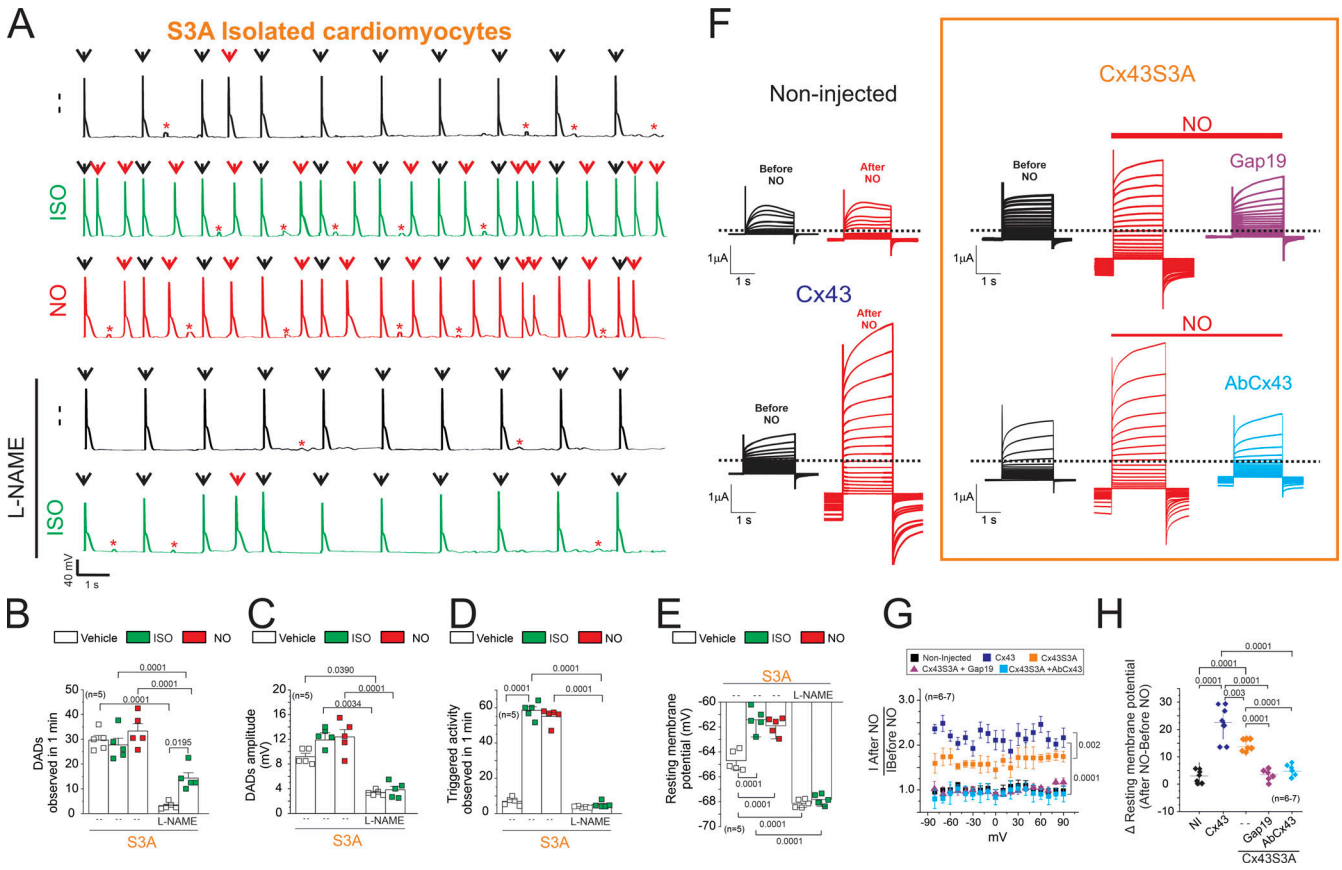

Figure 7. **β-adrenergic cardiac stress evokes triggered activity in S3A cardiac cells via S-nitrosylation of lateralized Cx43 hemichannels. (A)** Representative AP traces of S3A isolated cardiomyocytes. Cells were stimulated with 1 µM Iso in the presence of 100 µM L-NAME (NOS blocker) or 1 µM DEENO (NO donor). Arrow indicates electrical stimulation. Black arrows indicate electrical stimulation pulse. Red arrows indicate TAs. Red asterisks display DADs. **(B)** Quantification of DADs observed in A. P = 0.0001 S3A vs. S3A + L-NAME, P = 0.0001 S3A + Iso vs. S3A + ISO + L-NAME, P = 0.0195 S3A + L-NAME vs. S3A + L-NAME + Iso. Comparisons between groups were made using nested-ANOVA. The number in parentheses indicates biological replicates. We analyzed three to five cells per mouse. **(C)** Quantification of DADs amplitude observed in A. P = 0.0390 S3A vs. S3A + L-NAME, P = 0.0034 S3A + Iso vs. S3A + L-NAME, P = 0.0001 NO vs. S3A + L-NAME. Comparisons between groups were made using nested-ANOVA. The number in parentheses indicates biological replicates. We analyzed three to five cells per mouse. **(D)** Quantification of TA observed in A. P = 0.0001 S3A vs. S3A + Iso; P = 0.0001 S3A + Iso vs. S3A + Iso + L-NAME. Comparisons between groups were made using nested-ANOVA. The number in parentheses indicates biological replicates. We analyzed three to five cells per mouse. **(E)** Resting membrane potential of WT and S3A cardiomyocytes. P = 0.0001 S3A vs. S3A + Iso; P = 0.0001 vs. S3A vs. S3A + NO; P = 0.0001 S3A vs. S3A + L-NAME. Comparisons between groups were made using nested-ANOVA. The number in parentheses indicates biological replicates. We analyzed three to five cells per mouse. **(F)** Representative current traces before and after application of 10 µM DEENO in a non-injected oocyte or an oocyte expressing Cx43 and Cx43S3A. Oocytes were clamped to −80 mV, and square pulses from −80 mV to +90 mV (in 10 mV steps) were then applied for 2 s. At the end of each pulse, the membrane potential was returned to −80 mV. Intracellular injection of Gap19 (232 ng/µl) or a Cx43 CT antibody (2.5 ng/µl) reduces NO-induced Cx43 hemichannel currents. **(G)** Normalized currents were obtained from the ratio between recorded currents after and before DEENO treatment. The number in parentheses indicates biological replicate. We analyzed three to five oocytes per frog. P = 0.002 Cx43 vs. Cx43S3A; P = 0.0001 Cx43S3A vs. Cx43S3A + Gap19. Comparisons between groups were made using two-way ANOVA plus Tukey's post-hoc test. **(H)** Changes in resting membrane potential in the presence or absence of 10 µM DEENO. Cx43 hemichannel blockers restore normal resting membrane potential. Comparisons between groups were made using two-way ANOVA plus Tukey's post-hoc test.

dystrophic cardiomyopathy (Gutstein et al., 2001; Gollob, 2006; Bruce et al., 2008; Saffitz, 2009; Thibodeau et al., 2010; Remo et al., 2012; Gonzalez et al., 2018; Kim et al., 2019; Lillo et al., 2019; Himelman et al., 2020). Mechanisms linking Cx43 remodeling to the enhanced propensity for arrhythmic activity have been associated with the dysfunction of multiple cellular signaling pathways (Gollob, 2006; Saffitz et al., 2009; Thibodeau et al., 2010; Kim et al., 2019). Abnormal localization and/or gating of ion channels (including Nav1.5, NCX, and K^+ currents, among others) disturbs the highly organized temporal and spatial pattern of cardiac excitation. The resulting slow dysfunctional and often heterogeneous conduction favors reentrant activity, thus promoting arrhythmias, fibrillation, heart failure, or sudden death (Gollob, 2006; Saffitz et al., 2009; Thibodeau et al., 2010; Kim et al., 2019). However, among all these studies only a few have considered the role of Cx43 hemichannels as a mediator of arrhythmogenic behavior (Kim et al., 2019; Lillo et al., 2019; Himelman et al., 2020; De Smet et al., 2021; Lillo and Contreras, 2021).

We have previously demonstrated that β-adrenergic stimulation in dystrophic cardiomyocytes evoked TA and Ca^{2+} entry by opening S-nitrosylated Cx43 hemichannels (Gonzalez et al.,

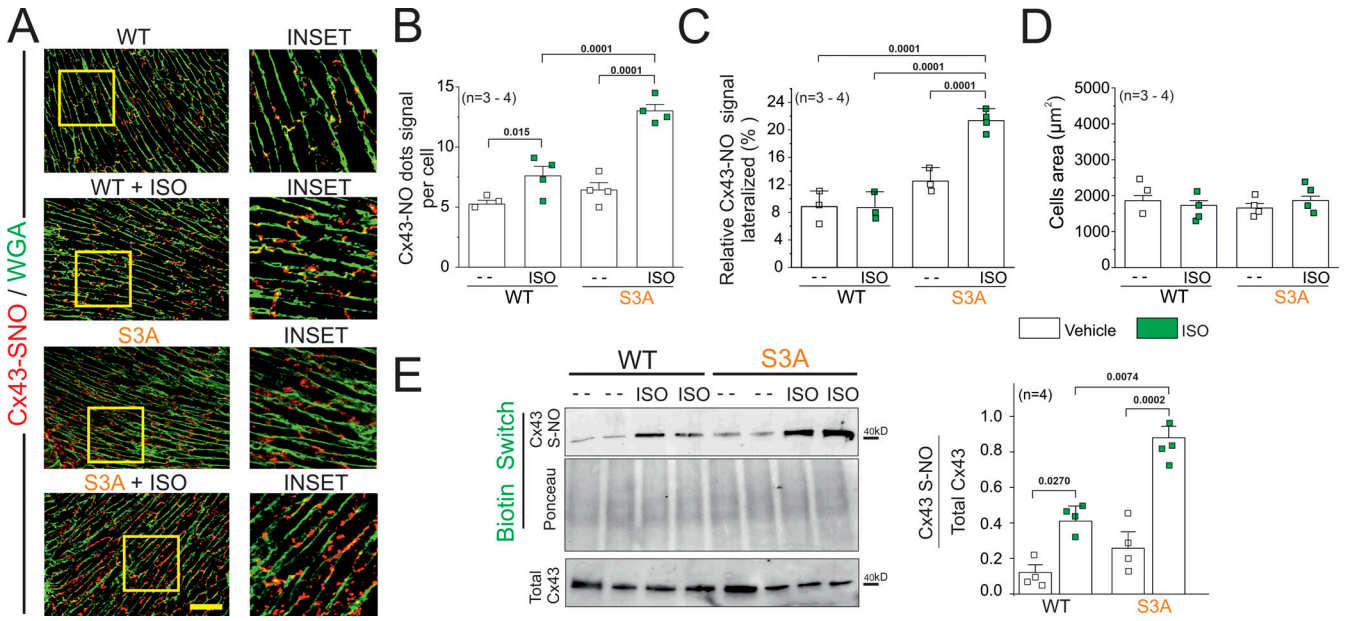

Figure 8. **β-adrenergic cardiac stress evokes S-nitrosylation lateralized Cx43 proteins. (A)** Representative images of analysis performed by PLA of the interaction between Cx43 and S-nitrosylation. Plasma membrane stained with wheat germ agglutinin (WGA) and S-nitrosylated Cx43 (Cx43-SNO) are shown in green and red, respectively. Scale bar: 50 µm. **(B)** Quantification of PLA dots signals observed in A. P = 0.015 WT vs. WT + Iso; P = 0.0001 WT + Iso vs. S3A + Iso; P = 0.0001 S3A vs. S3A + Iso. Comparisons between groups were made using two-way ANOVA plus Tukey's post-hoc test. The number in parentheses indicates biological replicate. **(C)** The relative percentage of Cx43-NO dots signal at the lateral side of cardiomyocytes detected in A. Note that S3A-Iso enhanced lateralized signal. P = 0.0001 WT vs. S3A + Iso; P = 0.0001 WT + Iso vs. S3A + Iso; P = 0.0001 S3A vs. S3A + Iso. Comparisons between groups were made using two-way ANOVA plus Tukey's post-hoc test. The number in parentheses indicates biological replicate. **(D)** Analysis of cell areas are detected in WT and S3A mice under a vehicle and upon Iso stimulation. **(E)** Top and middle gels were loaded with S-nitrosylated proteins pulled down using the biotin switch assay. The top gel was then blotted against Cx43. The middle gel is the corresponding ponceau staining. The lower blot was loaded using total cardiac proteins and blotted against Cx43 from heart samples blotted against Cx43. The bottom graph is the quantification for two independent blots using the ratio for SNO-Cx43/total Cx43. P = 0.0270 WT vs. WT + Iso; P = 0.0074 WT + Iso vs. S3A + Iso; P = 0.0002 S3A vs. S3A + Iso. Comparisons between groups were made using two-way ANOVA plus Tukey's post-hoc test. The number in parentheses indicates biological replicate. Source data are available for this figure: SourceData F8.

2018; Lillo et al., 2019; Himelman et al., 2020). TA and Ca^{2+} entry were prevented by Cx43 hemichannel blockers (Lillo et al., 2019; Himelman et al., 2020) or by genetically reducing levels of Cx43 in a dystrophic mouse model (Lillo et al., 2019). They were also prevented in dystrophic cardiac cells where Cx43 was genetically modified to prevent remodeling (Himelman et al., 2020). In line with these findings, a recent report showed that the blockade of Cx43 hemichannels in ventricular cardiomyocytes from heart failure patients prevents cardiac stress-induced spontaneous Ca^{2+} release, DADs, and TA (De Smet et al., 2021). In the present work, we showed that β-adrenergic stimulation results in depolarization of the cardiac plasma membrane in both WT and S3A cardiomyocytes. However, the depolarization of S3A cells was larger and evokes TA. Cx43 hemichannel blockers restored the resting membrane potential in Iso-treated S3A cardiomyocytes to levels observed in WT and significantly decreased TA. Similar to what was described by us in dystrophic cardiomyocytes (Lillo et al., 2019), Iso-treated S3A cardiomyocytes only produced a rightward shift of ~7 mV in the resting membrane potential compared with WT cells. We previously explained that severe changes in the resting membrane potential that would be caused by the full opening of Cx43 hemichannels are prevented by physiological extracellular Ca^{2+} concentration, which significantly decreases Cx43 hemichannel open probability (Contreras et al., 2003; Lillo et al., 2019).

Arrhythmogenic events in S3A mice were also detected in the absence of β-adrenergic stimulation mainly during the dark phase of the light/dark cycle (Fig. 2 B and Fig. S2), when mice were most active. Consistently, at the cellular level, we observed TA in isolated S3A cardiomyocytes without Iso-stimulation. Thus, both TA and arrhythmias are likely linked to sporadic increases of intracellular Ca^{2+} in cardiomyocytes. It is well known that dysregulation of Ca^{2+} handling promotes arrhythmogenic phenotypes in several animal models of heart failure (Gollob, 2006; Saffitz et al., 2009; Thibodeau et al., 2010; Kyrychenko et al., 2013; Gonzalez et al., 2018; Kim et al., 2019; Lillo et al., 2019; Himelman et al., 2020). Disruption of Ca^{2+} homeostasis leads to DADs, EADs, and TA. For instance, in plakophilin-2-2 (PKP2)-deficient mice, Cx43 hemichannel activity is upregulated, resulting in increased intracellular Ca^{2+} levels and, consequently, arrhythmogenic behavior (Kim et al., 2019). In this work, the authors suggest that Cx43 hemichannels at the surface membrane of cardiomyocytes might offer a pathway for Ca^{2+} entry into cardiomyocytes from PKP2-deficient mice. Hence, blockade of Cx43 hemichannels with Gap19 or using PKP2 mice with lower levels of Cx43 (PKP2: $Cx43^{+/-}$) leads to the rescue of Ca^{2+} homeostasis and reduction of membrane leakage to small molecules (evaluated by Lucifer yellow uptake)

in isolated hearts (Kim et al., 2019). Our current data in S3A cardiomyocytes are in line with these previous findings by showing that Ca^{2+} handling is significantly affected by Cx43 remodeling. This is sustained by the prolonged Ca^{2+} decay times observed in S3A cardiomyocytes when compared with WT cells. Normalization of Ca^{2+} decay time values in S3A cardiomyocytes by pretreatment with Gap19 suggests that the opening of remodeled Cx43 hemichannels might allow Ca^{2+} entry. Ethidium uptake assays further support the opening of remodeled Cx43 hemichannels by showing that Iso-treatment produced a substantial increase in membrane permeability of S3A hearts that is significantly reduced by the blockade of Cx43 hemichannels. We inferred that cardiac stress-induced Ca^{2+} dysfunction, DADs, and TA result from enhanced activity of Cx43 hemichannels in S3A cardiomyocytes.

β-Adrenergic or electrical cardiac stimulation activates cellular signaling pathways that include multiple enzymes such as Akt, PKA, Ca^{2+}/calmodulin-dependent protein kinase II, and NOS (Zhu et al., 2003; Grimm and Brown, 2010; Mani et al., 2010; Hegyi et al., 2019; Lillo et al., 2019). These pathways are responsible for the phosphorylation or S-nitrosylation of multiple cardiac ion channels (Vielma et al., 2016), including Cx43 proteins (Lillo et al., 2019). These posttranslational modifications modulate cardiac electrical activity and Ca^{2+} homeostasis (Zhu et al., 2003; Grimm and Brown, 2010; Thibodeau et al., 2010; Kyrychenko et al., 2013; Hegyi et al., 2019; Kim et al., 2019). Recent evidence indicates that cardiac Cx43 hemichannels under physiological conditions can open as a result of a moderate increase in intracellular Ca^{2+} directly following Iso-induced RyR2 activation (Lissoni et al., 2021). The data convincingly show a functional crosstalk between Cx43 and RyR2 receptors. In addition, Cx43 hemichannels were found interacting in microdomains with RyR2 at the ID, close to the perinexus. The authors reported that elevations of diastolic Ca^{2+} through caffeine or β-adrenergic-stimulation promoted the activity of single Cx43 hemichannels in isolated and paired ventricular cardiomyocytes in pigs and mice (De Smet et al., 2021). Interestingly, they also showed that further hemichannel opening evoked few DADs or TA in healthy cardiomyocytes.

Another feature that has been associated with arrhythmogenic behavior is the prolongation of APD (Tse, 2016). Consistently with previous results (Remo et al., 2011; Lillo et al., 2019; De Smet et al., 2021; Lissoni et al., 2021), our data indicate that Cx43 hemichannels modulate the duration of the AP in both WT cardiac cells and S3A. This observation was detected in other cardiac models, where Cx43 proteins are also remodeled. Ghazizadeh et al. (2020) reported, in an atrial fibrillation cardiac model, that inhibition of Cx43 hemichannels rescues the changes in APD and membrane leakage. By blocking Cx43 hemichannel activity, we restored the APD in cells with Cx43 lateralized hemichannels, such as Dystrophic cardiac cells (Lillo et al., 2019) or S3A isolated cells, with and without isoproterenol stimulation (Fig. 6). While we favor the idea that prolonged APD in isolated S3A cardiomyocytes might associate with Na^{+} and/or Ca^{2+} entry via the opening of Cx43 hemichannels, we cannot rule out, at this time, that lateralization of Cx43 proteins might also alter expression and/or function of Na^{2+} and Ca^{2+} channels, including the effect on late Na^{+} current or L-type Ca^{2+} current. Yet, our results strongly support the idea that Cx43 hemichannels activity modulates cardiac excitability in pathological cardiomyocytes and, perhaps, in healthy ones.

RyR2 is one of the most studied Ca^{2+} channels in cardiac pathologies. Dysregulation in phosphorylation or nitrosylation patterns modifies RyR2 activity and affects Ca^{2+} handling (Gonzalez et al., 2007; Forrester et al., 2009; Fauconnier et al., 2010; Lima et al., 2010), changing electrical cardiac performance and inducing heart arrhythmias, heart failure, or even sudden death in several cardiac animal models (Marx et al., 2000; Oxford et al., 2007; Fauconnier et al., 2010; Grimm and Brown, 2010; Mani et al., 2010; Remo et al., 2012; Kim et al., 2019; Lillo et al., 2019; Himelman et al., 2020). In dystrophic mice, both RyR2 and Cx43 become hypernitrosylated upon β-adrenergic stimulation (Fauconnier et al., 2010; Lillo et al., 2019; Vielma et al., 2020). Inhibition of NO production by L-NAME reduced S-nitrosylation of Cx43 hemichannels in dystrophic mice as well as the related increase in membrane depolarization and the development of TA and arrhythmias (Lillo et al., 2019). Similarly, in the hearts of S3A mice, Cx43 becomes highly S-nitrosylated in the lateral membrane of cardiomyocytes, and L-NAME treatment of isolated S3A cardiomyocytes diminished Cx43 hemichannel-mediated membrane depolarization and TA. We also confirmed that Cx43 S3A hemichannels are activated by NO when expressed in heterologous *Xenopus* oocytes, although the activation was slightly less than Cx43 WT. Yet, activation of Cx43 S3A hemichannels was sufficient to produce large membrane depolarizations in *Xenopus* oocytes. As expected, the activation of Cx43 S3A hemichannels was significantly inhibited when Gap19 or AbCx43 was injected into the oocytes. These inhibitors also restore changes in oocyte membrane potentials mediated by Cx43 S3A hemichannels in a similar manner to that observed in S3A cardiomyocytes. These controls validate a role for the opening of Cx43 hemichannels mediating changes in membrane excitability.

Importantly, our findings in the S3A knock-in mice support a pathological role for remodeled Cx43 hemichannels, which alter membrane excitability and enhance cardiomyocyte dysfunction upon cardiac stress. These findings may help to develop therapeutic approaches for multiple cardiomyopathy phenotypes where Cx43 proteins are remodeled.

Data availability

Data are available in the article and supplementary materials. Raw data are available from the authors upon reasonable request.

Acknowledgments

David A. Eisner served as editor.

We thank Dr. Glenn I. Fishman (New York University) for providing the original S3A founder mice for our colonies.

This work was supported by an American Heart Association (AHA) post-doctoral fellowship 18POST339610107 and an AHA Career Development Award 932684 to M.A. Lillo, AHA post-

doctoral fellowship 23POST1027462 to M. Muñoz, Muscular Dystrophy Association grant 416281 to D. Fraidenraich, NIH grant HL093342 to N. Shirokova, NIH grants R01HL92929 and R01Hl133294 to L.H. Xie, AHA grant 16GRNT31100022 to L.H.Xie, NIH grant 1R01HL141170-01 to D. Fraidenraich, N. Shirokova, and J.E. Contreras, and NIH grant 1R01GM099490 to J.E. Contreras.

Author contributions: M.A. Lillo, M. Muñoz, P. Rhana, K. Gaul-Muller, J. Quan, L.F. Santana, and J.E. Contreras, designed experiments. M.A. Lillo performed most of the experiments. M.A. Lillo, M. Muñoz, P. Rhana, J. Quan, L.-H. Xie, L.F. Santana, and J.E. Contreras analyzed the data. M.A. Lillo and J.E. Contreras wrote the original draft manuscript. M. Muñoz, N. Shirokova, L.F. Santana, and D. Fraidenraich edited the final manuscript. All authors reviewed and approved the final draft.

Disclosures: The authors declare no competing interests exist.

Submitted: 21 March 2022
Revised: 25 January 2023
Revised: 6 April 2023
Accepted: 24 April 2023

References

Abudara, V., J. Bechberger, M. Freitas-Andrade, M. De Bock, N. Wang, G. Bultynck, C.C. Naus, L. Leybaert, and C. Giaume. 2014. The connexin43 mimetic peptide Gap19 inhibits hemichannels without altering gap junctional communication in astrocytes. *Front. Cell. Neurosci.* 8:306. https://doi.org/10.3389/fncel.2014.00306

Bruce, A.F., S. Rothery, E. Dupont, and N.J. Severs. 2008. Gap junction remodelling in human heart failure is associated with increased interaction of connexin43 with ZO-1. *Cardiovasc. Res.* 77:757–765. https://doi.org/10.1093/cvr/cvm083

Contreras, J.E., J.C. Sáez, F.F. Bukauskas, and M.V. Bennett. 2003. Gating and regulation of connexin 43 (Cx43) hemichannels. *Proc. Natl. Acad. Sci. USA.* 100:11388–11393. https://doi.org/10.1073/pnas.1434298100

De Smet, M.A., A. Lissoni, T. Nezlobinsky, N. Wang, E. Dries, M. Pérez-Hernández, X. Lin, M. Amoni, T. Vervliet, K. Witschas, et al. 2021. Cx43 hemichannel microdomain signaling at the intercalated disc enhances cardiac excitability. *J. Clin. Invest.* 131:131. https://doi.org/10.1172/JCI137752

Ebihara, L. 1996. *Xenopus* connexin38 forms hemi-gap-junctional channels in the nonjunctional plasma membrane of *Xenopus* oocytes. *Biophys. J.* 71:742–748. https://doi.org/10.1016/S0006-3495(96)79273-1

Eisner, D.A. 2021. Pseudoreplication in physiology: More means less. *J. Gen. Physiol.* 153:e202012826. https://doi.org/10.1085/jgp.202012826

Fauconnier, J., J. Thireau, S. Reiken, C. Cassan, S. Richard, S. Matecki, A.R. Marks, and A. Lacampagne. 2010. Leaky RyR2 trigger ventricular arrhythmias in Duchenne muscular dystrophy. *Proc. Natl. Acad. Sci. USA.* 107:1559–1564. https://doi.org/10.1073/pnas.0908540107

Figueroa, X.F., M.A. Lillo, P.S. Gaete, M.A. Riquelme, and J.C. Sáez. 2013. Diffusion of nitric oxide across cell membranes of the vascular wall requires specific connexin-based channels. *Neuropharmacology*. 75:471–478. https://doi.org/10.1016/j.neuropharm.2013.02.022

Forrester, M.T., M.W. Foster, M. Benhar, and J.S. Stamler. 2009. Detection of protein S-nitrosylation with the biotin-switch technique. *Free Radic. Biol. Med.* 46:119–126. https://doi.org/10.1016/j.freeradbiomed.2008.09.034

Ghazizadeh, Z., T. Kiviniemi, S. Olafsson, D. Plotnick, M.E. Beerens, K. Zhang, L. Gillon, M.J. Steinbaugh, V. Barrera, and S.H.J.C. Sui. 2020. Metastable atrial state underlies the primary genetic substrate for MYL4 mutation-associated atrial fibrillation. *Circulation*. 141:301–312. https://doi.org/10.1161/CIRCULATIONAHA.119.044268

Gollob, M.H. 2006. Cardiac connexins as candidate genes for idiopathic atrial fibrillation. *Curr. Opin. Cardiol.* 21:155–158. https://doi.org/10.1097/01.hco.0000221574.95383.6f

Gonzalez, D.R., F. Beigi, A.V. Treuer, and J.M. Hare. 2007. Deficient ryanodine receptor S-nitrosylation increases sarcoplasmic reticulum calcium leak and arrhythmogenesis in cardiomyocytes. *Proc. Natl. Acad. Sci. USA.* 104:20612–20617. https://doi.org/10.1073/pnas.0706796104

Gonzalez, J.P., J. Ramachandran, E. Himelman, M.A. Badr, C. Kang, J. Nouet, N. Fefelova, L.H. Xie, N. Shirokova, J.E. Contreras, and D. Fraidenraich. 2018. Normalization of connexin 43 protein levels prevents cellular and functional signs of dystrophic cardiomyopathy in mice. *Neuromuscul. Disord.* 28:361–372. https://doi.org/10.1016/j.nmd.2018.01.012

Gonzalez, J.P., J. Ramachandran, L.H. Xie, J.E. Contreras, and D. Fraidenraich. 2015. Selective Connexin43 inhibition prevents isoproterenol-induced arrhythmias and lethality in muscular dystrophy mice. *Sci. Rep.* 5:13490. https://doi.org/10.1038/srep13490

Grimm, M., and J.H. Brown. 2010. β-adrenergic receptor signaling in the heart: Role of CaMKII. *J. Mol. Cell. Cardiol.* 48:322–330. https://doi.org/10.1016/j.yjmcc.2009.10.016

Gutstein, D.E., G.E. Morley, H. Tamaddon, D. Vaidya, M.D. Schneider, J. Chen, K.R. Chien, H. Stuhlmann, and G.I. Fishman. 2001. Conduction slowing and sudden arrhythmic death in mice with cardiac-restricted inactivation of connexin43. *Circ. Res.* 88:333–339. https://doi.org/10.1161/01.RES.88.3.333

Hegyi, B., S. Morotti, C. Liu, K.S. Ginsburg, J. Bossuyt, L. Belardinelli, L.T. Izu, Y. Chen-Izu, T. Bányász, E. Grandi, and D.M. Bers. 2019. Enhanced depolarization drive in failing rabbit ventricular myocytes: Calcium-dependent and β-adrenergic effects on late sodium, L-type calcium, and sodium-calcium exchange currents. *Circ. Arrhythm. Electrophysiol.* 12:e007061. https://doi.org/10.1161/CIRCEP.118.007061

Himelman, E., M.A. Lillo, J. Nouet, J.P. Gonzalez, Q. Zhao, L.H. Xie, H. Li, T. Liu, X.H. Wehrens, P.D. Lampe, et al. 2020. Prevention of connexin-43 remodeling protects against Duchenne muscular dystrophy cardiomyopathy. *J. Clin. Invest.* 130:1713–1727. https://doi.org/10.1172/JCI128190

Huang, R.Y., J.G. Laing, E.M. Kanter, V.M. Berthoud, M. Bao, H.W. Rohrs, R.R. Townsend, and K.A. Yamada. 2011. Identification of CaMKII phosphorylation sites in Connexin43 by high-resolution mass spectrometry. *J. Proteome Res.* 10:1098–1109. https://doi.org/10.1021/pr1008702

Johnson, R.G., H.C. Le, K. Evenson, S.W. Loberg, T.M. Myslajek, A. Prabhu, A.M. Manley, C. O'Shea, H. Grunenwald, M. Haddican, et al. 2016. Connexin hemichannels: Methods for dye uptake and leakage. *J. Membr. Biol.* 249:713–741. https://doi.org/10.1007/s00232-016-9925-y

Kim, J.-C., M. Pérez-Hernández, F.J. Alvarado, S.R. Maurya, J. Montnach, Y. Yin, M. Zhang, X. Lin, C. Vasquez, and A.J.C. Heguy. 2019. Disruption of $Ca^{2+}{}_i$ homeostasis and connexin 43 hemichannel function in the right ventricle precedes overt arrhythmogenic cardiomyopathy in Plakophilin-2–deficient mice. *Circulation*. 140:1015–1030. https://doi.org/10.1161/CIRCULATIONAHA.119.039710

Kleber, A.G., and J.E. Saffitz. 2014. Role of the intercalated disc in cardiac propagation and arrhythmogenesis. *Front. Physiol.* 5:404. https://doi.org/10.3389/fphys.2014.00404

Kyrychenko, S., E. Poláková, C. Kang, K. Pocsai, N.D. Ullrich, E. Niggli, and N. Shirokova. 2013. Hierarchical accumulation of RyR post-translational modifications drives disease progression in dystrophic cardiomyopathy. *Cardiovasc. Res.* 97:666–675. https://doi.org/10.1093/cvr/cvs425

Lillo, M.A., and J.E. Contreras. 2021. Opening the floodgates: An emerging role for Connexin-43 hemichannels in the heart. *Cell Calcium*. 97:102410. https://doi.org/10.1016/j.ceca.2021.102410

Lillo, M.A., E. Himelman, N. Shirokova, L.H. Xie, D. Fraidenraich, and J.E. Contreras. 2019. S-nitrosylation of connexin43 hemichannels elicits cardiac stress-induced arrhythmias in Duchenne muscular dystrophy mice. *JCI Insight*. 4:e130091. https://doi.org/10.1172/jci.insight.130091

Lima, B., M.T. Forrester, D.T. Hess, and J.S. Stamler. 2010. S-nitrosylation in cardiovascular signaling. *Circ. Res.* 106:633–646. https://doi.org/10.1161/CIRCRESAHA.109.207381

Lissoni, A., P. Hulpiau, T. Martins-Marques, N. Wang, G. Bultynck, R. Schulz, K. Witschas, H. Girao, M. De Smet, and L. Leybaert. 2021. RyR2 regulates Cx43 hemichannel intracellular Ca^{2+}-dependent activation in cardiomyocytes. *Cardiovasc Res.* 117:123–136. https://doi.org/10.1093/cvr/cvz340

López-Cano, M., V. Fernández-Dueñas, and F. Ciruela. 2019. Proximity ligation assay image analysis protocol: Addressing receptor-receptor interactions. *Methods Mol. Biol.* 2040:41–50. https://doi.org/10.1007/978-1-4939-9686-5_3

Mani, S.K., E.A. Egan, B.K. Addy, M. Grimm, H. Kasiganesan, T. Thiyagarajan, L. Renaud, J.H. Brown, C.B. Kern, and D.R. Menick. 2010. β-Adrenergic receptor stimulated Ncx1 upregulation is mediated via a CaMKII/AP-

1 signaling pathway in adult cardiomyocytes. *J. Mol. Cell. Cardiol.* 48: 342–351. https://doi.org/10.1016/j.yjmcc.2009.11.007

Marx, S.O., S. Reiken, Y. Hisamatsu, T. Jayaraman, D. Burkhoff, N. Rosemblit, and A.R. Marks. 2000. PKA phosphorylation dissociates FKBP12.6 from the calcium release channel (ryanodine receptor): Defective regulation in failing hearts. *Cell.* 101:365–376. https://doi.org/10.1016/S0092-8674(00)80847-8

Oxford, E.M., H. Musa, K. Maass, W. Coombs, S.M. Taffet, and M. Delmar. 2007. Connexin43 remodeling caused by inhibition of plakophilin-2 expression in cardiac cells. *Circ. Res.* 101:703–711. https://doi.org/10.1161/CIRCRESAHA.107.154252

Pfeiffer, S., E. Leopold, K. Schmidt, F. Brunner, and B. Mayer. 1996. Inhibition of nitric oxide synthesis by NG-nitro-L-arginine methyl ester (L-NAME): Requirement for bioactivation to the free acid, NG-nitro-L-arginine. *Br. J. Pharmacol.* 118:1433–1440. https://doi.org/10.1111/j.1476-5381.1996.tb15557.x

Qu, J., F.M. Volpicelli, L.I. Garcia, N. Sandeep, J. Zhang, L. Márquez-Rosado, P.D. Lampe, and G.I. Fishman. 2009. Gap junction remodeling and spironolactone-dependent reverse remodeling in the hypertrophied heart. *Circ. Res.* 104:365–371. https://doi.org/10.1161/CIRCRESAHA.108.184044

Remo, B.F., S. Giovannone, and G.I. Fishman. 2012. Connexin43 cardiac gap junction remodeling: Lessons from genetically engineered murine models. *J. Membr. Biol.* 245:275–281. https://doi.org/10.1007/s00232-012-9448-0

Remo, B.F., J. Qu, F.M. Volpicelli, S. Giovannone, D. Shin, J. Lader, F.Y. Liu, J. Zhang, D.S. Lent, G.E. Morley, and G.I. Fishman. 2011. Phosphatase-resistant gap junctions inhibit pathological remodeling and prevent arrhythmias. *Circ. Res.* 108:1459–1466. https://doi.org/10.1161/CIRCRESAHA.111.244046

Rossow, C.F., K.W. Dilly, C. Yuan, M. Nieves-Cintrón, J.L. Cabarrus, and L.F. Santana. 2009. NFATc3-dependent loss of I_{to} gradient across the left ventricular wall during chronic β adrenergic stimulation. *J. Mol. Cell. Cardiol.* 46:249–256. https://doi.org/10.1016/j.yjmcc.2008.10.016

Saffitz, J.E. 2009. Desmosome mutations in arrhythmogenic right ventricular cardiomyopathy: Important insight but only part of the picture. *Circ. Cardiovasc. Genet.* 2:415–417. https://doi.org/10.1161/CIRCGENETICS.109.909366

Saffitz, J.E., A. Asimaki, and H. Huang. 2009. Arrhythmogenic right ventricular cardiomyopathy: New insights into disease mechanisms and diagnosis. *J. Investig. Med.* 57:861–864. https://doi.org/10.2310/JIM.0b013e3181c5e631

Severs, N.J., S.R. Coppen, E. Dupont, H.I. Yeh, Y.S. Ko, and T. Matsushita. 2004a. Gap junction alterations in human cardiac disease. *Cardiovasc. Res.* 62:368–377. https://doi.org/10.1016/j.cardiores.2003.12.007

Severs, N.J., E. Dupont, S.R. Coppen, D. Halliday, E. Inett, D. Baylis, and S. Rothery. 2004b. Remodelling of gap junctions and connexin expression in heart disease. *Biochim. Biophys. Acta.* 1662:138–148. https://doi.org/10.1016/j.bbamem.2003.10.019

Severs, N.J., E. Dupont, N. Thomas, R. Kaba, S. Rothery, R. Jain, K. Sharpey, and C.H. Fry. 2006. Alterations in cardiac connexin expression in cardiomyopathies. *Adv. Cardiol.* 42:228–242. https://doi.org/10.1159/000092572

Söderberg, O., M. Gullberg, M. Jarvius, K. Ridderstråle, K.J. Leuchowius, J. Jarvius, K. Wester, P. Hydbring, F. Bahram, L.G. Larsson, and U. Landegren. 2006. Direct observation of individual endogenous protein complexes in situ by proximity ligation. *Nat. Methods.* 3:995–1000. https://doi.org/10.1038/nmeth947

Thibodeau, I.L., J. Xu, Q. Li, G. Liu, K. Lam, J.P. Veinot, D.H. Birnie, D.L. Jones, A.D. Krahn, R. Lemery, et al. 2010. Paradigm of genetic mosaicism and lone atrial fibrillation: Physiological characterization of a connexin 43-deletion mutant identified from atrial tissue. *Circulation.* 122:236–244. https://doi.org/10.1161/CIRCULATIONAHA.110.961227

Tse, G. 2016. Mechanisms of cardiac arrhythmias. *J. Arrhythm.* 32:75–81. https://doi.org/10.1016/j.joa.2015.11.003

Vielma, A.Z., M.P. Boric, and D.R. Gonzalez. 2020. Apocynin treatment prevents cardiac connexin 43 hemichannels hyperactivity by reducing nitroso-redox stress in mdx mice. *Int. J. Mol. Sci.* 21:5415. https://doi.org/10.3390/ijms21155415

Vielma, A.Z., L. León, I.C. Fernández, D.R. González, and M.P. Boric. 2016. Nitric oxide synthase 1 modulates basal and β-adrenergic-stimulated contractility by rapid and reversible redox-dependent S-nitrosylation of the heart. *PLoS One.* 11:e0160813. https://doi.org/10.1371/journal.pone.0160813

Wang, N., E. De Vuyst, R. Ponsaerts, K. Boengler, N. Palacios-Prado, J. Wauman, C.P. Lai, M. De Bock, E. Decrock, M. Bol, et al. 2013. Selective inhibition of Cx43 hemichannels by Gap19 and its impact on myocardial ischemia/reperfusion injury. *Basic Res. Cardiol.* 108:309. https://doi.org/10.1007/s00395-012-0309-x

Zhu, W.-Z., S.-Q. Wang, K. Chakir, D. Yang, T. Zhang, J.H. Brown, E. Devic, B.K. Kobilka, H. Cheng, and R.-P.J.T.J.o.c.i. Xiao. 2003. Linkage of β 1-adrenergic stimulation to apoptotic heart cell death through protein kinase A–independent activation of Ca^{2+}/calmodulin kinase II. *J Clin Invest.* 111:617–625. https://doi.org/10.1172/JCI16326

Supplemental material

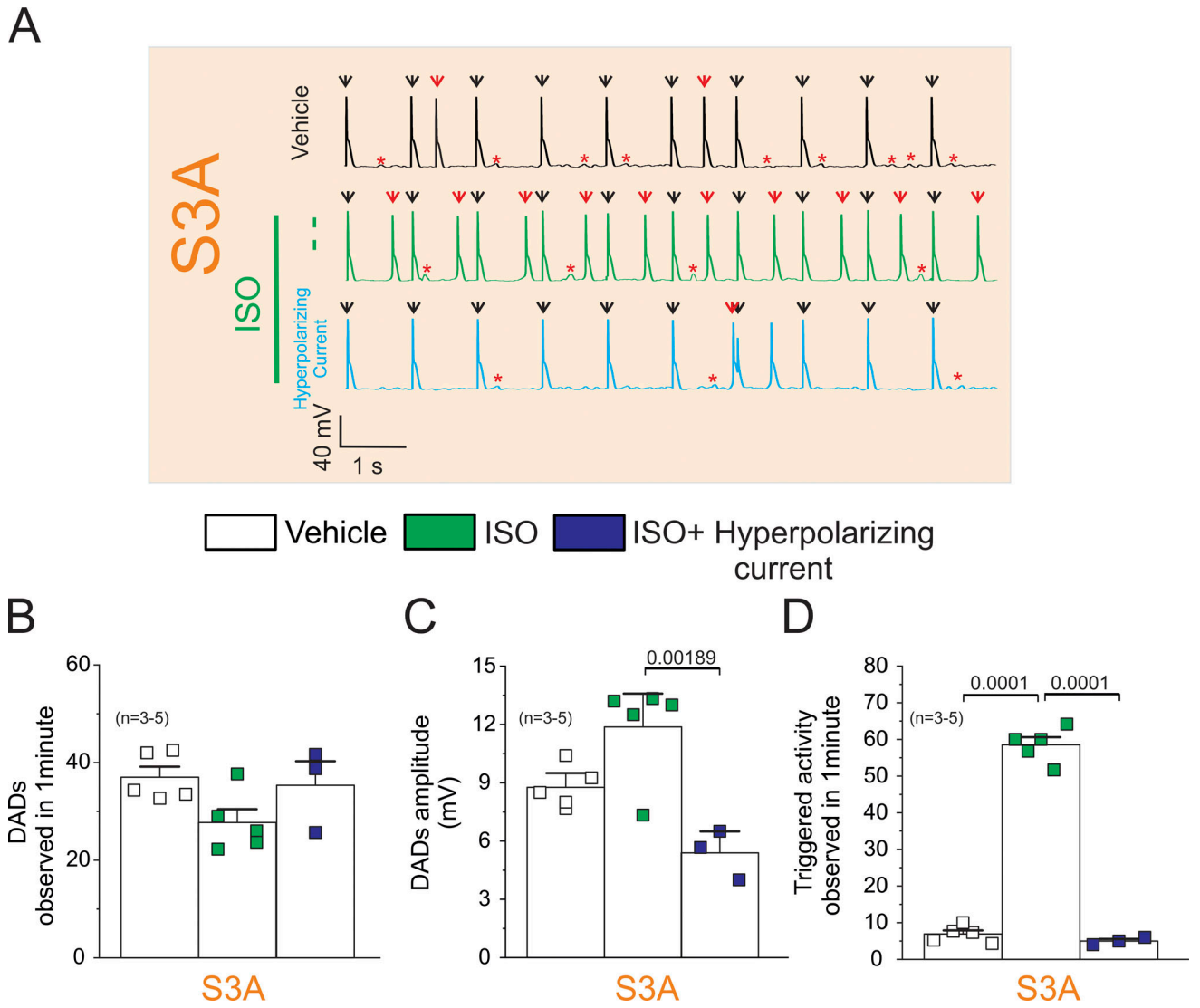

Figure S1. **Injection of hyperpolarizing current is sufficient to regulate DAD and TA in isolated S3A cardiomyocytes. (A)** Representative APs traces of S3A isolated cardiomyocytes in the absence or presence of 1 µM Iso. Hyperpolarizing currents (20–12 pA) were injected to maintain the resting membrane potential close to −68 mV (value observed in WT cardiomyocytes). Black arrows indicate electrical stimulation pulse. Red arrows indicate TAs. Red asterisks display DADs. **(B)** Quantification of DADs observed in 1 min. **(C)** Quantification of DADs amplitude. **(D)** Quantification of TAs detected in 1 min. The number in parentheses indicates biological replicates. Comparisons between groups were made using nested-ANOVA plus Tukey's post-hoc test.

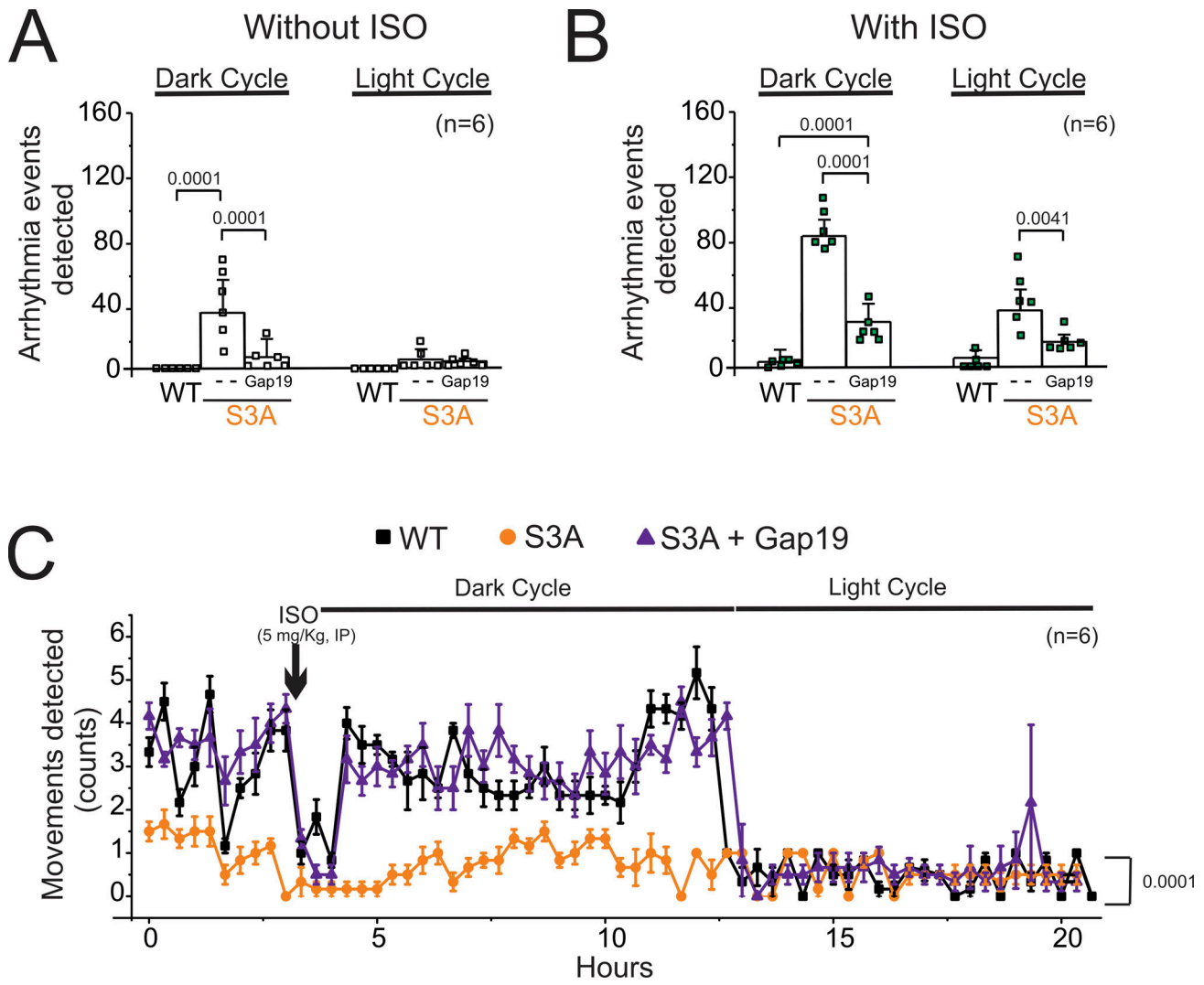

Figure S2. **S3A mice displayed arrhythmogenic behaviors during the dark cycle with and without Iso. (A)** Quantification of arrhythmogenic events (including PVC, double PVC, VT, or AV block) from 4–6-mo-old mice during the dark and light cycle without Iso in WT, S3A, and S3A mice treated with Gap19 via retroorbital injection (10 µg/kg). The number in parentheses indicates the *n* value. Comparisons between groups were made using two-way ANOVA plus Tukey's post-hoc test. **(B)** Quantification of arrhythmogenic events (including PVC, double PVC, VT, or AV block) from 4–6-mo-old mice during the dark and light cycle upon Iso stimulation (5 mg/kg, IP) in WT, S3A, and S3A mice treated with Gap19 via retroorbital injection (10 µg/kg). The number in parentheses indicates biological replicate. Comparisons between groups were made using two-way ANOVA plus Tukey's post-hoc test. **(C)** Movements were detected using an in vivo telemetry system in WT, S3A, and S3A mice treated with Gap19 via retroorbital injection (10 µg/kg). Arrow indicates Iso stimulation. Comparisons between groups were made using two-way ANOVA plus Tukey's post-hoc test.